frontiers in Earth Science

ORIGINAL RESEARCH
published: 11 January 2019
doi: 10.3389/feart.2018.00247

Insights Into the Mechanisms of Phreatic Eruptions From Continuous High Frequency Volcanic Gas Monitoring: Rincón de la Vieja Volcano, Costa Rica

Angelo Battaglia[1], J. Maarten de Moor[2], Alessandro Aiuppa[1], Geoffroy Avard[2], Henriette Bakkar[3], Marcello Bitetto[1], M. M. Mora Fernández[4,5], Peter Kelly[6], Gaetano Giudice[7], Dario Delle Donne[1] and Hairo Villalobos[2]*

[1] Dipartimento DiSTeM, Università di Palermo, Palermo, Italy, [2] Observatorio Vulcanológico y Sismológico de Costa Rica, Universidad Nacional, Heredia, Costa Rica, [3] ICE, Sabana Norte, San José, Costa Rica, [4] Escuela Centroamericana de Geología, Universidad de Costa Rica, San José, Costa Rica, [5] Red Sismológica Nacional (RSN: UCR-ICE), Universidad de Costa Rica, San José, Costa Rica, [6] United States Geological Survey, Cascades Volcano Observatory, Vancouver, DC, United States, [7] Sezione di Palermo, Istituto Nazionale di Geofisica e Vulcanologia, Palermo, Italy

OPEN ACCESS

Edited by:
Jacob B. Lowenstern, Volcano Disaster Assistance Program (USGS), United States

Reviewed by:
Hiroshi Shinohara, Geological Survey of Japan (AIST), Japan
Paul Wallace, University of Oregon, United States

***Correspondence:**
Angelo Battaglia
angelo.battaglia03@unipa.it

Specialty section:
This article was submitted to Volcanology, a section of the journal Frontiers in Earth Science

Received: *26 June 2018*
Accepted: *18 December 2018*
Published: *11 January 2019*

Citation:
Battaglia A, de Moor JM, Aiuppa A, Avard G, Bakkar H, Bitetto M, Mora Fernández MM, Kelly P, Giudice G, Delle Donne D and Villalobos H (2019) Insights Into the Mechanisms of Phreatic Eruptions From Continuous High Frequency Volcanic Gas Monitoring: Rincón de la Vieja Volcano, Costa Rica. Front. Earth Sci. 6:247. doi: 10.3389/feart.2018.00247

Understanding the trigger mechanisms of phreatic eruptions is key to mitigating the effects of these hazardous but poorly forecastable volcanic events. It has recently been established that high-rate volcanic gas observations are potentially very suitable to identifying the source processes driving phreatic eruptions, and to eventually detecting precursory changes prior to individual phreatic blasts. In February-May 2017, we deployed a Multi-GAS instrument to continuously monitor gas concentrations in the crater lake plume of Rincón de la Vieja, a remote and poorly monitored active volcano in Costa Rica, site of frequent phreatic/phreatomagmatic eruptions. Forty-two phreatic/phreatomagmatic eruptions were seismically recorded during our investigated period, 9 of which were also recorded for gas by the Multi-GAS. To the best of our knowledge, these represent the first instrumentally measured gas compositions during individual phreatic/phreatomagmatic explosions at an active volcano. Our results show that during background quiescent degassing the Rincón de la Vieja crater lake plume was characterized by high CO_2/SO_2 ratios of 64 ± 59 and H_2S/SO_2 ratios of 0.57 ± 0.20. This composition is interpreted as reflecting hydrothermal (re)processing of magma-sourced gas in the sub-limnic environment. Phreatic blasts were recorded by the Multi-GAS as brief (1–2 min long) pulses of elevated gas mixing ratios (up to ~52 ppmv SO_2 and >3,000 ppmv CO_2), or more than an order of magnitude higher than during background degassing (~1 ppmv SO_2 and ~450 ppmv CO_2). During the phreatic eruption(s), the H_2S/SO_2 ratio was systematically lower (<0.18) than during background degassing, but the CO_2/SO_2 ratio remained high (and variable), ranging from 37 to 390. These S-poor compositions for the eruptive gas imply extensive processing of the source magmatic gas during pre-eruptive hydrothermal storage, likely by deposition of native S and/or sulfate. Our gas results are thus overall consistent with a mechanism of phreatic eruptions

triggered by accumulation of magmatic-hydrothermal gases beneath a hydrothermal seal. We claim that real-time Multi-GAS monitoring is urgently needed at other crater lake-hosting volcanoes (e.g., Ruapehu, Aso), where phreatic eruptions may similarly be preceded by phases of reduced S degassing at the surface.

Keywords: volcanic gases, crater lakes, Rincón de la Vieja, phreatic eruption, Multi-GAS, Costa Rica

INTRODUCTION

Phreatic eruptions are among the most unpredictable and hazardous volcanic phenomena (Mastin and Witter, 2000; Browne and Lawless, 2001). These blasts involve the violent, explosive discharge of pressurized pockets of external (non-volcanic, mostly meteoric) water, and are therefore particularly common at "wet" volcanoes whose summits are topped by crater lakes (Rouwet and Morrissey, 2015; Stix and de Moor, 2018). In addition to the large availability of exogenous water, active crater lakes are especially prone to developing phreatic eruptions owing to the presence of a persistent heat source (conductive/convective heating from shallow magma, and/or rising magmatic volatiles), and the frequent formation of permeability barriers at the lake bottom (e.g., impermeable layers of precipitated native sulfur or alteration minerals) that favor gas accumulation (Christenson et al., 2010; Christenson and Tassi, 2015; Delmelle and Bernard, 2015, and references cited therein). The exact mechanisms driving crater lake breaching eruptions are still not entirely understood, and the respective roles of the magmatic and sublimnic hydrothermal systems in triggering the eruptions are still a matter of debate (Takano et al., 1994; Christenson and Tassi, 2015; Rouwet and Morrissey, 2015).

Phreatic eruptions have typically occurred in the past without being preceded by any obvious precursor, as recently dramatically demonstrated by the deadly Ontake (in 2014, Oikawa et al., 2016) and Kusatsu-Shirane (in 2018) eruptions in Japan. The recent technical advances in real-time observation of lake plume gas compositions (Di Napoli et al., 2013; Shinohara et al., 2015; Tamburello et al., 2015; de Moor et al., 2016a; Gunawan et al., 2016) bring a new perspective on eruption forecasting. Using measurements from a permanently installed "lake" Multi-GAS (Multi-component Gas Analyser System; Aiuppa et al., 2006, 2010; Aiuppa, 2015), de Moor et al. (2016a) identified for the first time systematic short-term (days to weeks) variations in plume gas compositions prior to individual phreatic explosions at Laguna Caliente crater lake, Poás volcano (Costa Rica). These observations indicated an increase of magmatic volatiles input prior to individual phreatic blasts, which demonstrates the potential of high-frequency real-time gas monitoring.

Here, we report on the results of 3 months of instrumental monitoring of volcanic gas composition at Rincón de la Vieja volcano (10.49 N, 85.19 W), in the Costa Rican segment of the Central American volcanic arc (CAVA). Rincón de la Vieja is one of the most active and remote volcanoes in Costa Rica (Barquero and Segura, 1983; Alvarado et al., 1992), and hosts a highly acidic crater lake (Tassi et al., 2005, 2009), the source of recurrent phreatomagmatic to phreatic eruptions (Boudon et al., 1996). The intense (SO_2 > 60 tons/day; de Moor et al., 2017) gas emissions have only occasionally been studied in the past (Tassi et al., 2005, 2009; Aiuppa et al., 2014; de Moor et al., 2017), due to the limited accessibility of the volcano summit. Our study here provides the first near-continuous gas dataset taken during a period of recurrent phreatic activity at Rincon de la Vieja, including the first measurement of the syn-explosive gas phase. The aim is to use our novel gas observations to derive new insights into the mechanisms driving crater lake phreatic explosions and assess the potential for forecasting eruptions at Rincón de la Vieja.

RINCÓN DE LA VIEJA VOLCANO

Rincón de la Vieja volcano is part of the Guanacaste volcanic range (**Figure 1**), a Quaternary magmatic range related to subduction of the Cocos plate underneath the Caribbean plate (Carr, 1984; Carr et al., 1990; DeMets, 2001; DeMets et al., 2010). The Guanacaste volcanic range consists of four andesitic central edifices (Orosí-Cacao, Rincón de la Vieja-Santa María, Miravalles, and Tenorio-Montezuma). Before construction of the Quaternary andesitic chain, intense explosive silicic volcanism generated a series of collapse events and associated calderas (Molina et al., 2014). The Rincón de la Vieja-Santa María volcanic complex (maximum elevation 1,916 m) was constructed within one of these calderas, the 120 km^2 Cañas Dulces Caldera (Molina and Martí, 2016). The Cañas Dulce caldera hosts several hydrothermal fields (Giggenbach and Correales, 1992), including several thermal manifestations on the Rincón de la Vieja massif itself (Tassi et al., 2005), aligned along a NW-SE trend running roughly parallel to the volcano's axis.

Rincón de la Vieja (10.49 N, 85.19 W) is the only currently active andesitic stratovolcano in the Guanacaste Cordillera. The volume of the massif is estimated at 130 km^3 (Carr, 1984). The most recent magmatic eruption (with significant juvenile component) took place ∼3,500 years B.P. (Alvarado et al., 1992). This eruption left the dacitic Rio Blanco tephra deposit (volume, 0.25 km^3), which also includes a small fraction (<3%) of andesitic scoria and pumice indicating a mixed magma reservoir (Kempter, 1997). The historically active crater has produced frequent phreatic to phreatomagmatic eruptions since 1851 (Boudon et al., 1996). Major eruptions in the mid-1990s caused large lahars and significant damage to local communities. The 1995, 1991, 1983, 1967, 1966, and 1922 eruptions expelled part of the crater lake, producing acidic lahars (Barquero and Segura, 1983; OVSICORI, 1995; Kempter, 1997; Kempter and Rowe, 2000), mostly breaching through the topographically lower northern crater rim.

FIGURE 1 | Structural and volcanological setting of the Costa Rica segment of the Central American Volcanic Arc (CAVA). Modified from Brandes et al. (2007). Map data: Google, Landsat/Copernicus image, SIO, NOAA, U.S. Navy, NGA, GEBCO.

Rincón de la Vieja is monitored by Observatorio Vulcanológico y Sismológico de Costa Rica-Universidad Nacional (OVSICORI-UNA) and the Instituto Costaricense de Electricidad (ICE). Volcano monitoring is complicated by remote location and extreme field conditions (high rainfall, frequent fog and extremely windy). The active crater today hosts a large hyper-acidic lake (pH = 0.7–1 and T = 26–30°C in February-March 2017) (**Figure 2**), characterized by vigorous degassing and continuous overturning (Tassi et al., 2005, 2009; de Moor et al., 2017). Dark-gray spherules of colloidal sulfur are widespread on the lake's surface (**Figure 2**), while fumarolic emissions up to 130°C are observed on the inner crater walls (Tassi et al., 2005; Aiuppa et al., 2014).

Phreatic/phreatomagmatic activity resumed in September 2011, after 13 years of quiescence. During 2012–2013, Rincón de la Vieja exhibited low seismicity and very infrequent eruptions. From September 2014, eruptive activity escalated to an average of 25 phreatic-phreatomagmatic events per month, peaking in October 2015 and March 2016 when 43 and 220 eruptions were recorded, respectively. Visual binocular microscope observations (made by G. Avard at OVSICORI-UNA, following the procedure described in Alvarado et al., 2016) revealed that erupted ash fragments (250–500 μm portion) contain well-preserved greenish minerals and a small portion (~5%) of fresh-looking glassy and vesicular shards. These observations were interpreted as indicative of the involvement of shallow magma in 2015–2016, as is the case at many volcanoes with phreatic eruptions (e.g., Stix and de Moor, 2018). Native sulfur fragments were also systematically observed in the erupted products of 2015–2017, especially in the 1–2 mm ash grain-size fraction (G. Avard, pers. comm.). Sulfur-rich minerals were also repeatedly observed as veins and fillings in fractures of large ejecta and blocks dispersed throughout the crater. The frequency and seismic energy of eruptions increased in early 2017. During our gas monitoring interval (February 3–May 9, 2017) 42 seismic signals associated to phreatic/phreatomagmatic eruptions were recognized, and 9 of these eruptions were also identified geochemically (**Table 1**; see below). Some of these 9 eruptions (eruptions 1–3 and 9; **Figure 3**) were preceded by a long period (LP) seismic signal several seconds before the explosion. In almost all cases (eruptions 1, 3, 4–7), pulses of spasmodic tremor occurred a few hours before the eruption. Two major phreatic/phreatomagmatic eruptions (generating hot lahars that traveled outside the crater to the north) took place on May 23 and on June 11 (Global Volcanism Program, 2017), just a few weeks after our Multi-GAS stopped acquiring. The explosion on June 11 generated a 1–2 km high plume, and ejected coarse materials to the W and NW onto the upper N flank. This event, the largest (based on seismic energy) registered during 2011–2018, was preceded by a LP swarm 2 h before the explosion. Material collected from the May 23 lahar down the river contained only ~1% juvenile component, but fragments erupted from the June 11 eruption (also collected from a lahar) contained ~44% juvenile material (OVSICORI-UNA). Phreatic activity has intermittently continued until the time of writing (late 2018).

MATERIALS AND METHODS

The gas dataset we report on in this study was recorded using two distinct fully autonomous Multi-GAS instruments, one

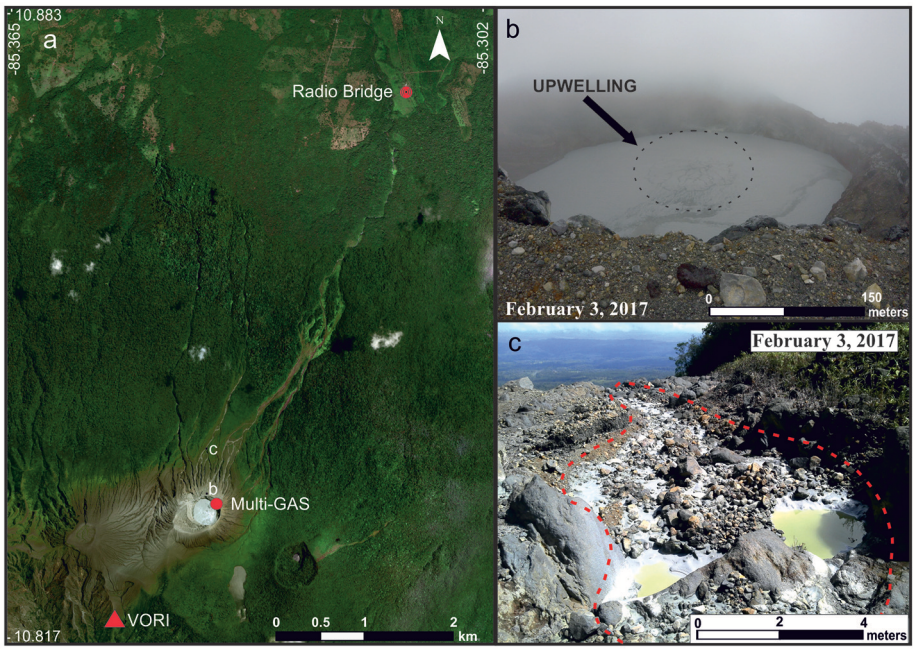

FIGURE 2 | (a) Satellite image of Rincón de la Vieja volcano showing location of the Multi-GAS measurement site, the VORI seismic station, and the Radio Bridge, map data: Google, Landsat/Copernicus image, SIO, NOAA, U.S. Navy, NGA, GEBCO; **(b)** The Rincón de la Vieja active crater, with convection cells and abundant gray sulfur spherules floating on the lake surface; **(c)** Water and sulfur deposits in a canyon on the northern slope of Rincón de la Vieja.

designed by the Instituto Nazionale di Geofisica e Vulcanologia (INGV) and one designed by the U.S. Geological Survey (USGS). The two instruments (INGV and USGS-campaign) operated sequentially at the same site, located on the northern inner wall of the active crater ∼1 m downwind the lake shore (Lat. 10.8327 Long. −85.3355; see **Figure 2**). This site was selected because its position ensured regular fumigation by the lake gas plume, while minimizing any potential gas contribution from low-temperature crater fumaroles (not observed at the measurement site during our study). The Multi-GAS instruments were powered by an external (12 V, 40 Ah) battery and 3 solar panels in order to ensure proper operation in all climatic conditions. A PVC tube with two filters served as gas inlet, and allowed gas to be pumped (at 1.2 L/m) inside the Multi-GAS instruments. The first (INGV-type) Multi-GAS was installed on February 3, 2017 and operated until March 17, 2017, when it was dismantled (for use at a different volcano) and replaced by a second (USGS-campaign type; Gunawan et al., 2016) Multi-GAS. This latter operated until May 09, 2017, when it stopped transmitting data before being finally destroyed during the May 23 lahar-producing phreatic blast (Global Volcanism Program, 2017).

The two Multi-GAS instruments used very similar sensor kits (see below) and were re-calibrated at OVSICORI with the same standard gases before the installation, showing very similar response. The INGV-type Multi-GAS was recalibrated after returning from the field (in late March 2017), and the original calibration was reproduced within sensor precision. Both Multi-GAS instruments measured SO_2 and H_2S mixing ratios (precision within ± 15% at 2σ; Lewicki et al., 2017) with the same specific electrochemical sensors (models TD2G-1A and TC4E-1A, respectively; all from City Technology and with ± 5% repeatability). Interference of SO_2 gas on the H_2S sensor (15 %) was determined during calibration procedure and corrected with the Ratiocalc software. CO_2 mixing ratios were measured using an on-board spectrometer (INGV-type: Gascard EDI030102NG, measurement range = 0–3,000 ppmv, precision, ± 3% at 2σ; USGS-type LI-COR LI-840A, measurement range = 0–5,000 ppmv, precision, ± 1.5% at 2σ). The INGV-type Multi-GAS instrument, controlled by an arduino2 datalogger, acquired data at 0.1 Hz rate during 4 sampling periods per day, of 30 min duration each. In the USGS-type Multi-GAS, all data acquisition and scheduling was controlled by a Campbell Scientific data logger (CR1000 with NL115 module) outfitted with 2 GB of onboard memory. The station completed four data acquisition cycles per day, in which data were acquired for 1 h at a 1 Hz rate. Before and after each measurement cycle, the station performed sensor baseline checks by activating two miniature 3-way teflon solenoid valves (Cole-Parmer WU-01540-11) that formed a closed-loop and recirculated trapped sample gases through soda lime and desiccant for 3 min to remove acid gases and water vapor in order to provide a measure of within-run baseline drift and to clean and dry the instrument prior to shutting down. For both Multi-GAS instruments, data were telemetered (at the end of each acquisition cycle) via radio modem (Xetawave) to OVSICORI using a radio bridge installed on the northern base of the volcano (**Figure 2**). The acquired gas mixing ratios data were post-processed using the Ratiocalc software (Tamburello,

TABLE 1 | Time (in GMT), duration (in s), and associated energy (in J) of the phreatic-phreatomagmatic eruptions occurring during February-May 2017.

Date	Time eruption (GMT)	Duration (s)	Seismic energy (J)	Multi-GAS peak time (GMT)	Eruption number
05/02/2017	7:47:50	42	18.42		
07/02/2017	12:53:06	52	56.03		
07/02/2017	18:19:29	72	28.67		
08/02/2017	22:44:32	61	48.58		
09/02/2017	17:49:41	51	7.74		
13/02/2017	2:59:04	16	9.16		
13/02/2017	9:16:49	138	9.69	9:12:06 - 9:16:35	1
14/02/2017	17:47:42	62	5.96		
16/02/2017	7:12:50	112	42.73		
16/02/2017	13:27:24	173	20.07		
19/02/2017	1:56:00	88	12.86		
19/02/2017	5:49:24	198	7.38		
20/02/2017	15:22:06	106	17.43	15:23:04	2
23/02/2017	3:34:16	94	7.80	03:34:50	3
25/02/2017	12:56:36	106	8.42		
26/02/2017	5:30:48	175	16.94		
27/02/2017	n/a	n/a	n/a	03:16:20	4
02/03/2017	21:24:35	n/a	n/a	21:25:56 – 21:26:50	5
11/03/2017	22:49:17	342	18.88		
14/03/2017	20:53:19	155	8.69		
18/03/2017	23:34:14	272	50.12		
20/03/2017	n/a	n/a	n/a	06:16:00	6
20/03/2017	19:03:50	227	73.83		
26/03/2017	10:11:07	174	18.73		
26/03/2017	10:28:39	115	54.56		
26/03/2017	10:55:42	88	52.67		
26/03/2017	15:49:39	124	80.15		
27/03/2017	10:15:39	70	26.25		
29/03/2017	9:31:17	253	23.58		
31/03/2017	12:46:49	n/a	40.95		
31/03/2017	14:10:50	n/a	38.31		
04/04/2017	14:48:20	122	24.00		
04/04/2017	15:03:49	90	128.66		
06/04/2017	7:48:06	606	103.30		
12/04/2017	17:46:18	175	48.14	17:53:00	7
19/04/2017	0:38:16	200	234.62		
19/04/2017	1:49:19	195	89.22		
20/04/2017	00:02:00	n/a	n/a	00:05:00	8
23/04/2017	5:12:41	111	9.74		
25/04/2017	6:18:40	114	11.47	06:21:00	9
28/04/2017	1:26:16	381	46.28		
09/05/2017	14:59:47	312	24.02		

Nine of these eruptions were also recorded by the Multi-GAS (the "Multi-GAS peak Time" identifies the temporal window of Multi-GAS over which the syn-explosive gas was detected). The nine eruptions are numbered as in ***Figure 3****.*

2015) to derive gas ratios between volatile couples (CO_2/SO_2 and H_2S/SO_2) using linear regression. In order to derive accurate gas ratios, the different response time (∼2–4 s) between the spectroscopic sensor and the electrochemical sensors was corrected for during data processing with the Ratiocalc software. No pressure correction was applied to the electrochemical sensors owing to very similar altitude between calibration site (Heredia, ∼1,200 m) and Rincon's summit (∼1,500 m). Based on laboratory tests with standard gases, errors in the derived ratios are typically ≤15%. Unfortunately, the plume was condensing at all conditions encountered during observations, so it was not possible to determine a robust volcanic H_2O signal.

Seismic activity was characterized using the reference station VORI, operated by the Observatorio Sismológico y Vulcanológico de Arenal y Miravalles (OSIVAM) of the Instituto Costarricense de Electricidad (ICE). This station is located 1.8 km

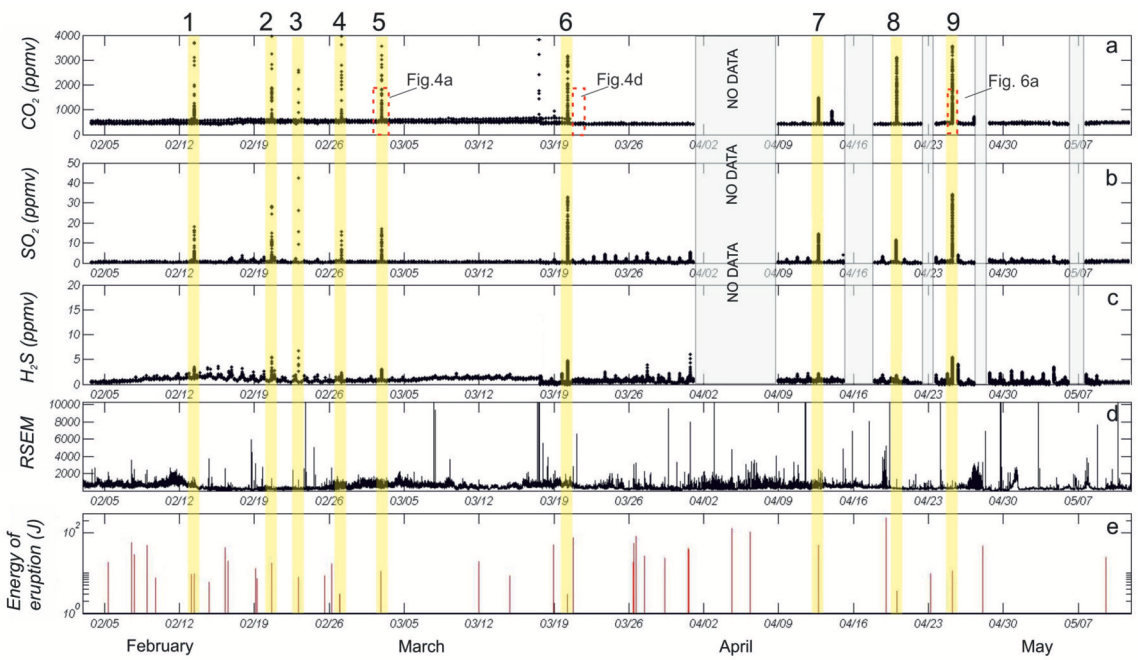

FIGURE 3 | Time-series of **(a–c)** gas mixing ratios (in ppmv); **(d)** RSEM, **(e)** eruptive energy. Note that Multi-GAS data (CO_2, SO_2, and H_2S mixing ratios) are not continuous but obtained during 4 daily cycles, each 30–60 min long. The shaded yellow bands identify the 9 explosions (numbered #1 to #9) during which the Multi-GAS was operating, allowing the *syn-explosive* gas composition to be determined. The five light gray areas identify all periods with no MultiGAS data. The small red insets in the CO_2 plot identify the expanded portions shown in **Figures 4**, **6**.

SW of the active crater, and is equipped with a digital 3-component broadband TRIMBLE REFTEK 151B sensor with flat response from 0.016 (60 s) to 50 Hz. Signals were sampled at 100 Hz. Close inspection of seismic records was carried out to extract discrete events and, in the particular case of eruptive signals, to estimate the associated seismic energy ($E_{seismic}$). Seismic energy was calculated using the relation for bodywaves generated by an isotropic source at the top of a homogeneous half space (Boatwright, 1980; Arámbula-Mendoza et al., 2011):

$$E_{seismic} = 2\pi r^2 \rho_{earth} c_{earth} \frac{1}{A} \int S^2 U(t)^2 dt \quad (1)$$

where r is the distance from the source to the seismic station, ρ is rock density, c is the P wave velocity, S is the site effect, U is seismic amplitude and A is attenuation. We used $r = 1{,}800$ m, $c = 1{,}500$ m/s, $\rho = 2{,}600$ kg/m^3. The site and attenuation effects were neglected for simplicity.

The temporal evolution of seismic activity was explored using Real-time Seismic Energy Measurement, or RSEM (De la Cruz-Reyna and Reyes-Davila, 2001), which considers the square of the amplitude (directly related to seismic energy). The seismic signal was filtered in the band of 1–10 Hz in order to avoid strong ambient noise present in the records.

RESULTS

Figure 3 is a temporal record of CO_2, SO_2, and H_2S concentrations measured by the two Multi-GAS instruments. The RSEM time-series is shown in **Figure 3d** for comparison, along with **Figure 3e** the timing of each of the seismically-identified phreatic explosions.

The temporal plots exhibit a sequence of gas peaks (numbered #1 to #9 in **Figure 3**) that clearly emerge above a persistent background (characterized by low concentration of all gases). By comparison with seismic data (**Figures 3d,e**, **4a**), we find that each of the gas peaks corresponds to a Multi-GAS recording of a phreatic explosion, i.e., the peaks are records of the composition of the gas released during a phreatic blast (referred as *syn-explosive gas*). CO_2 and SO_2 (**Figures 3a,b**, **4a**) exhibit the most pronounced peaks in the *syn-explosive gas*, with peak concentrations of >3,000 ppmv and ∼52 ppmv, respectively. H_2S peaks are more moderate (typically < 5 ppmv).

Nine (**Figure 3**) of the 42 phreatic events that occurred during February 3-May 9, 2017 are captured by our Multi-GAS record (the remaining explosions took place outside the four daily Multi-GAS acquisition cycles). The background gas mixing ratios thus correspond to continuous passive degassing between the explosions, in what we refer to as the *quiescent gas*. The *quiescent gas* is typically characterized by low SO_2 and H_2S mixing ratios (<2 ppmv), and CO_2 (<500 ppmv) slightly above atmospheric background values.

As in other recent work (Aiuppa et al., 2017, 2018; de Moor et al., 2017), the Multi-GAS-derived gas mixing ratios data are post-processed to calculate the ratios between the various volatiles using the procedure of Tamburello (2015).

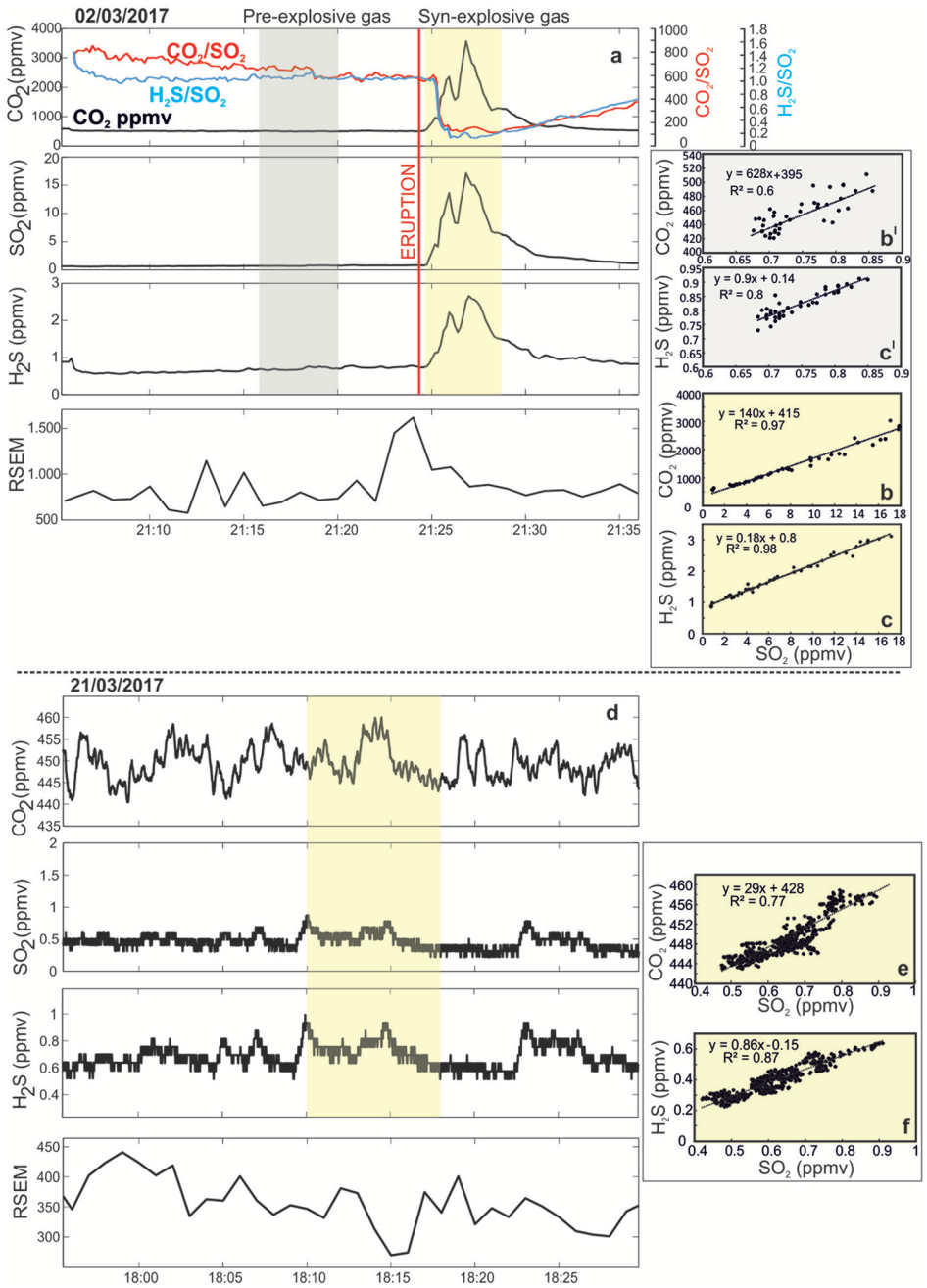

FIGURE 4 | (a) Detail of gas and seismic records taken on March 02, 2017 between ~21:05 and ~21:35 GMT. The eruption (event #5 in **Figure 3**, see inset) occurred at ~21:24 GMT. Mixing ratios increase after the blast, starting at ~21:24 GMT. The yellow-colored area corresponds to the sub-interval (identified with Ratiocalc) where CO_2, SO_2, and H_2S are positively correlated at statistically significant level ($R^2 > 0.6$). These subsets of CO_2, SO_2, and H_2S mixing ratios are used to draw **(b)** CO_2 vs. SO_2 and **(c)** H_2S vs. SO_2 correlation plots, and to calculate the time-averaged CO_2/SO_2 and H_2S/SO_2 ratios (within the yellow-colored temporal windows) from the slopes of the best-fit regression lines (listed in **Table 2**). In **(a)** the red and blue lines are high-resolution (1 Hz) records of CO_2/SO_2 and H_2S/SO_2 ratios, respectively, calculated by taking the ratio of individual couples of co-acquired mixing ratios. This point-to-point ratios (e.g., Pering et al., 2014) have large (~ 50 %) associated errors at the ppm level [e.g., before the explosion, **(a)**], so they should only be viewed as semi-quantitative estimates. Nevertheless, the contrasting gas signatures for *pre-explosive* and *syn-explosive gas* are clearly observed. Example of CO_2 vs. SO_2 and H_2S vs. SO_2 correlation plots for the *pre-explosive gas* [built from data within the gray-colored temporal windows in **(a)**], shown in **(b')** and **(c')**, confirm a very CO_2-rich (or SO_2-poor) gas composition prior to the blast. Gas ratios progressively return to the pre-eruptive levels toward the end of the Multi-GAS acquisition. **(d)** Example of gas and seismic records taken during a quiescent phase (March 21, 2017 between ~17:55 and ~18:30 GMT). Very low gas mixing ratios are observed throughout, as characteristic of the *quiescent gas*. The yellow-colored area corresponds to the only sub-interval (identified with Ratiocalc) where CO_2, SO_2, and H_2S are positively correlated at statistically significant level ($R^2 > 0.6$). These subsets of CO_2, SO_2, and H_2S mixing ratios are used to construct **(e)** CO_2 vs. SO_2 and **(f)** H_2S vs. SO_2 correlation plots, from which the time-averaged CO_2/SO_2 and H_2S/SO_2 ratios (within the yellow-colored temporal windows) are calculated (listed in **Table 2**).

To this aim, the gas mixing ratios time-series are sequentially examined with Ratiocalc to identify individual temporal windows (of ≥250 s, corresponding to subsets of ≥ 30 data points) with high correlation coefficients ($R^2 > 0.6$) between gas couples.

The procedure is illustrated in **Figures 4a,d** are temporal plots of mixing ratios recorded during a single explosion (**Figures 4a–c**), and during a typical quiescent degassing phase (**Figures 4d–f**) (see insets in **Figure 4**). By sequentially scanning the two sub-datasets, we identify the temporal intervals where the best correlations ($R^2 > 0.6$) between gas mixing ratio pairs are observed (yellow bands in **Figures 4a,d**). These subsets of CO_2, SO_2, and H_2S mixing ratios are then used to build CO_2 vs. SO_2 (**Figures 4b,e**) and H_2S vs. SO_2 (**Figures 4c,f**) correlation plots, and to calculate the time-averaged CO_2/SO_2 and H_2S/SO_2 ratios (within the yellow-colored temporal windows) from the slopes of the best-fit regression lines. The procedure is repeated for the entire dataset, and all the obtained gas ratio pairs are listed in **Table 2**.

Our gas ratios, listed in **Table 2** and illustrated in **Figure 5**, show contrasting H_2S/SO_2 ratios composition for the *quiescent gas* and the *syn-explosive gas*. The *quiescent gas* composition is characterized by H_2S/SO_2 ratios of 0.57 ± 0.2 (1 σ) (range, 0.01–1.5), or well above the H_2S/SO_2 of the gas released during the phreatic eruptions. This *syn-explosive gas* exhibits H_2S/SO_2 ratios of 0.04 ± 0.06 (range, 0.0003–0.18) (**Figure 5**). The *quiescent gas* H_2S/SO_2 ratio exhibits a weak but appreciable declining trend, from February (∼1) to early May (∼0.5) (**Figure 5B**), but remains systematically above the *syn-explosive gas* range (which shows no systematic trend).

Table 2 shows that *quiescent gas* and *syn-explosive gas* released by the lake have overlapping CO_2/SO_2 ratio compositions (64 ± 59 and 136 ± 110 at 1σ; **Figure 5A**). Both show a tendency of decreasing CO_2/SO_2 ratios from February (∼120 ± 51) to early May (∼70 ± 20).

Prior to each individual explosion, the CO_2, SO_2, and H_2S mixing ratios are typically very low (see **Figures 4a**, **6a**). Thus, the composition of the *quiescent gas* released in the minutes/seconds before an explosion, here refereed as *pre-explosive gas*, is not well constrained. One important aspect is, however, that the compositional change from *pre-explosive gas* to *syn-explosive gas* is large and abrupt at the onset of eruption (**Figures 4a**, **6a**). To highlight this observation, we show in **Figure 4a** the CO_2/SO_2 and H_2S/SO_2 ratios calculated by simply taking the ratio of individual couples of co-acquired mixing ratios. This point-to-point ratio approach (e.g., Pering et al., 2014) provides high-resolution (1 Hz) records of CO_2/SO_2 and H_2S/SO_2 ratios, see **Figures 4a**, **6a**. The errors associated with this methodology are potentially very large (∼ 50%, as based on laboratory tests) at the few ppm level (e.g., before the explosions), so the ratios displayed in **Figures 4a**, **6a** should only be viewed as semi-quantitative estimates. However, for the specific example shown in **Figure 4a**, the ratios calculated with the point-to-point ratio technique (respectively of 640 and 1.1 for CO_2/SO_2 and H_2S/SO_2) are reasonably close to those obtained with the scatter plot methodology described above (respectively of 628 and 0.9 for CO_2/SO_2 and H_2S/SO_2). A comparable similarity of point-to-point-derived and scatter plot-derived ratios is obtained for the explosion detailed in **Figure 6a** (see **Table 2**). We thus argue that the abrupt changes in CO_2/SO_2 and H_2S/SO_2 ratios at eruption onsets (**Figures 4a,e**, **6a**) are real, and point to very distinct gas signatures for *pre-explosive gas* and *syn-explosive gas*, with the former being typically more SO_2-poor. Very similar abrupt variations in gas ratios are observed for all 9 recorded explosions, followed by a gradual return to *quiescent gas* compositions over timescales of minutes (**Figures 4a**, **6a**). The point-to-point-derived compositions of the *pre-explosive gas* are listed in **Table 2**.

DISCUSSION

Our Multi-GAS results, in tandem with previous results (Aiuppa et al., 2014; de Moor et al., 2017), constrain the composition of the gas plume released by the Rincón de la Vieja crater lake (**Figure 7**). Our 2017 results confirm that SO_2 is the prevalent S gas species in the Rincón de la Vieja crater lake plume during both quiescent and explosive degassing, with H_2S/SO_2 <1 in all except six cases (**Table 2**). This is in line with previous reports (all Multi-Gas measurements) of Aiuppa et al. (2014) (1 survey in April 2013; H_2S/SO_2 = 0.9 ± 0.15) and (de Moor et al., 2017) (3 surveys between April 2014 and March 2016; H_2S/SO_2 of 0.05–0.3) (**Figure 7**). In contrast, low-temperature (<80°C) fumaroles, scattered on the inner crater walls, and around the lake shore, typically exhibit high H_2S/SO_2 ratios of ∼4 (Tassi et al., 2005). In these weaker hydrothermal manifestations, S re-equilibration (e.g., SO_2 conversion to H_2S) during cooling and reaction with wall-rocks in the fumarole's feeding conduits is very likely. Similarly, de Moor et al. (2016b) showed that Poas fumaroles have higher H_2S/SO_2 than the plume from the acid crater lake.

The 2017 crater lake plume is richer in CO_2 (CO_2/SO_2 ratios of 64 ± 59 to 136 ± 110 for *quiescent gas* and *syn-explosive gas, respectively*) than in 2013 (CO_2/SO_2 = 27 ± 15; Aiuppa et al., 2014) and 2014–2016 (CO_2/SO_2 of 4.3–9.5; de Moor et al., 2017) (a period over which Rincón's activity was progressively intensifying) (**Figure 7**). Thus, degassing at Rincón de la Vieja appears to be highly dynamic on yearly time scales in terms of gas compositions. Our continuous record from 2017 has much improved temporal resolution than past (campaign) surveys, and thus allows evaluation of the extent to which gas composition responds to high-frequency changes in volcanic activity. Three key observations emerge:

i) the plume H_2S/SO_2 ratio varied little during quiescent lake degassing in 2017: 0.57 ± 0.20 (**Figures 5B**, **7**); this limited variability is suggestive of S speciation buffering by fluid + solid phase reaction(s) (at least partially) (Giggenbach, 1987, 1996);
ii) during phreatic blasts, the gas emissions shift to more oxidized conditions (H_2S/SO_2 <0.18) than during quiescent degassing (**Figures 5B**, **6**); the compositional change at the eruption

TABLE 2 | Multi-GAS-derived (molar) CO_2/SO_2 and H_2S/SO_2 ratios in the Rincon de la Vieja crater lake plume.

Time	Ratio	Ratio value	R^2	Ratio	Ratio value	R^2	SO_2max (ppmv)	Eruption number
04/02/2017 09:05	CO_2/SO_2	100	0.65	H_2S/SO_2	0.54	0.62	0.68	
05/02/2017 03:05	CO_2/SO_2	115	0.68	H_2S/SO_2	0.69	0.65	0.70	
05/02/2017 09:05	CO_2/SO_2	109	0.67	H_2S/SO_2	1.07	0.60	0.69	
06/02/2017 03:05	CO_2/SO_2	102	0.65	H_2S/SO_2	0.75	0.70	0.67	
06/02/2017 21:05	CO_2/SO_2	137	0.70	H_2S/SO_2	0.83	0.68	0.67	
10/02/2017 21:05	CO_2/SO_2	193	0.64	H_2S/SO_2	0.91	0.63	0.63	
13/02/2017 09:08	CO_2/SO_2	502		H_2S/SO_2	1.03	0.94	0.66	PRE-EXPL
13/02/2017 09:12	CO_2/SO_2	131	0.78	H_2S/SO_2	0.0003	0.84	18.17	1
13/02/2017 15:05	CO_2/SO_2	99	0.70	H_2S/SO_2	0.61	0.75	0.86	
14/02/2017 09:05	CO_2/SO_2	51	0.70	H_2S/SO_2	0.82	0.70	0.97	
14/02/2017 15:05	CO_2/SO_2	320	0.65	H_2S/SO_2	0.94	0.68	0.59	
15/02/2017 03:05	CO_2/SO_2	90	0.64	H_2S/SO_2	0.65	0.60	0.58	
17/02/2017 03:05	CO_2/SO_2	198	0.60	H_2S/SO_2	0.74	0.64	0.47	
17/02/2017 15:05	CO_2/SO_2	118	0.62	H_2S/SO_2	0.37	0.70	1.08	
17/02/2017 21:05	CO_2/SO_2	38	0.65	H_2S/SO_2	0.43	0.65	3.71	
18/02/2017 15:05	CO_2/SO_2	144	0.60	H_2S/SO_2	0.52	0.60	1.52	
18/02/2017 21:05	CO_2/SO_2	59	0.65	H_2S/SO_2	0.49	0.62	2.34	
19/02/2017 21:05	CO_2/SO_2	41	0.65	H_2S/SO_2	0.41	0.67	3.16	
20/02/2017 03:05	CO_2/SO_2	101	0.68	H_2S/SO_2	0.46	0.63	0.87	
20/02/2017 15:17	CO_2/SO_2	567		H_2S/SO_2	0.40	0.79	1.08	PRE-EXPL
20/02/2017 15:23	CO_2/SO_2	99	0.82	H_2S/SO_2	0.08	0.93	28.38	2
20/02/2017 21:05	CO_2/SO_2	33	0.65	H_2S/SO_2	0.45	0.92	2.98	
21/02/2017 15:05	CO_2/SO_2	84	0.63	H_2S/SO_2	0.70	0.94	1.60	
21/02/2017 21:05	CO_2/SO_2	59	0.81	H_2S/SO_2	0.44	0.83	1.06	
22/02/2017 03:05	CO_2/SO_2	232	0.75	H_2S/SO_2	0.86	0.97	0.49	
22/02/2017 15:05	CO_2/SO_2	101	0.80	H_2S/SO_2	0.74	0.84	1.02	
22/02/2017 21:05	CO_2/SO_2	246	0.75	H_2S/SO_2	0.22	0.90	2.19	
23/02/2017 03:12	CO_2/SO_2	1296		H_2S/SO_2	1.30	0.60	0.40	PRE-EXPL
23/02/2017 03:34	CO_2/SO_2	38	0.68	H_2S/SO_2	0.0003	0.86	52.61	3
23/02/2017 15:05	CO_2/SO_2	113	0.62	H_2S/SO_2	1.06	0.75	1.14	
23/02/2017 21:05	CO_2/SO_2	118	0.65	H_2S/SO_2	0.90	0.86	1.00	
24/02/2017 15:05	CO_2/SO_2	167	0.74	H_2S/SO_2	1.17	0.84	0.96	
24/02/2017 21:05	CO_2/SO_2	95	0.69	H_2S/SO_2	0.36	0.90	1.99	
25/02/2017 15:05	CO_2/SO_2	286	0.65	H_2S/SO_2	1.54	0.80	0.59	
26/02/2017 03:05	CO_2/SO_2	62	0.70	H_2S/SO_2	0.54	0.83	1.08	
27/02/2017 03:11	CO_2/SO_2	730		H_2S/SO_2	0.90	0.89	0.75	PRE-EXPL
27/02/2017 03:16	CO_2/SO_2	231	0.97	H_2S/SO_2	0.010	0.89	15.70	4
28/02/2017 21:05	CO_2/SO_2	204	0.98	H_2S/SO_2	0.64	0.83	0.97	
02/03/2017 15:05	CO_2/SO_2	105	0.70	H_2S/SO_2	0.91	0.78	0.79	
02/03/2017 21:16	CO_2/SO_2	640 (628)	0.60	H_2S/SO_2	1.1 (0.9)	0.82	0.85	PRE-EXPL
02/03/2017 21:25	CO_2/SO_2	140	0.97	H_2S/SO_2	0.18	0.98	17.14	5
03/03/2017 21:05	CO_2/SO_2	216	0.68	H_2S/SO_2	0.85	0.80	0.70	
11/03/2017 03:05	CO_2/SO_2	86	0.85	H_2S/SO_2	0.92	0.89	0.74	
12/03/2017 21:05	CO_2/SO_2	118	0.82	H_2S/SO_2	0.63	0.85	0.95	
14/03/2017 21:05	CO_2/SO_2	62	0.70	H_2S/SO_2	0.90	0.84	0.91	
15/03/2017 03:05	CO_2/SO_2	217	0.75	H_2S/SO_2	0.97	0.86	0.70	
17/03/2017 17:58	CO_2/SO_2	67	0.66	H_2S/SO_2	0.56	0.66	0.60	
17/03/2017 23:57	CO_2/SO_2	38	0.63	H_2S/SO_2	0.97	0.74	0.44	
18/03/2017 00:20	CO_2/SO_2	270	0.70	H_2S/SO_2	0.53	0.60	0.45	
18/03/2017 11:59	CO_2/SO_2	170	0.65	H_2S/SO_2	0.86	0.63	0.45	

(Continued)

TABLE 2 | Continued

Time	Ratio	Ratio value	R^2	Ratio	Ratio value	R^2	SO_2max (ppmv)	Eruption number
18/03/2017 12:02	CO_2/SO_2	106	0.62	H_2S/SO_2	0.88	0.75	0.45	
18/03/2017 12:21	CO_2/SO_2	50	0.62	H_2S/SO_2	0.75	0.63	0.53	
18/03/2017 17:55	CO_2/SO_2	82	0.61	H_2S/SO_2	0.74	0.61	0.54	
18/03/2017 23:59	CO_2/SO_2	98	0.64	H_2S/SO_2	0.62	0.62	0.73	
19/03/2017 00:03	CO_2/SO_2	86	0.52	H_2S/SO_2	1.05	0.77	0.63	
19/03/2017 05:58	CO_2/SO_2	93	0.69	H_2S/SO_2	0.51	0.76	0.45	
19/03/2017 06:16	CO_2/SO_2	167	0.62	H_2S/SO_2	0.43	0.62	0.53	
19/03/2017 06:19	CO_2/SO_2	115	0.61	H_2S/SO_2	0.78	0.73	0.64	
19/03/2017 12:07	CO_2/SO_2	103	0.67	H_2S/SO_2	0.56	0.63	0.64	
19/03/2017 12:14	CO_2/SO_2	39	0.61	H_2S/SO_2	0.66	0.89	0.73	
19/03/2017 00:27	CO_2/SO_2	116	0.68	H_2S/SO_2	0.66	0.60	0.50	
19/03/2017 12:19	CO_2/SO_2	83	0.60	H_2S/SO_2	0.78	0.72	0.50	
19/03/2017 18:14	CO_2/SO_2	37	0.63	H_2S/SO_2	0.66	0.94	0.80	
20/03/2017 06:13	CO_2/SO_2	1265	0.98	H_2S/SO_2	0.81	0.60	0.44	PRE-EXPL
20/03/2017 06:16	CO_2/SO_2	70	0.98	H_2S/SO_2	0.004	0.99	32.80	6
21/03/2017 18:14	CO_2/SO_2	29	0.77	H_2S/SO_2	0.86	0.90	0.90	
23/03/2017 00:17	CO_2/SO_2	30	0.68	H_2S/SO_2	0.63	0.70	0.70	
24/03/2017 12:19	CO_2/SO_2	69	0.61	H_2S/SO_2	0.50	0.75	0.70	
26/03/2017 00:25	CO_2/SO_2	18	0.74	H_2S/SO_2	0.50	0.69	0.90	
26/03/2017 00:27	CO_2/SO_2	10	0.68	H_2S/SO_2	0.57	0.94	1.00	
27/03/2017 00:17	CO_2/SO_2	11	0.64	H_2S/SO_2	0.56	0.93	1.01	
27/03/2017 12:19	CO_2/SO_2	12	0.61	H_2S/SO_2	0.46	0.83	0.85	
28/03/2017 06:17	CO_2/SO_2	32	0.79	H_2S/SO_2	0.20	0.74	0.80	
28/03/2017 18:25	CO_2/SO_2	32	0.61	H_2S/SO_2	0.43	0.79	1.00	
29/03/2017 00:10	CO_2/SO_2	43	0.61	H_2S/SO_2	0.46	0.97	0.50	
29/03/2017 00:26	CO_2/SO_2	10	0.69	H_2S/SO_2	0.51	0.96	1.40	
30/03/2017 18:09	CO_2/SO_2	15	0.62	H_2S/SO_2	0.61	0.76	1.02	
30/03/2017 18:24	CO_2/SO_2	44	0.65	H_2S/SO_2	0.71	0.79	0.50	
31/03/2017 00:12	CO_2/SO_2	17	0.64	H_2S/SO_2	0.57	0.85	0.61	
31/03/2017 00:29	CO_2/SO_2	32	0.71	H_2S/SO_2	0.57	0.92	1.10	
31/03/2017 06:24	CO_2/SO_2	32	0.75	H_2S/SO_2	0.89	0.74	0.77	
31/03/2017 18:06	CO_2/SO_2	79	0.68	H_2S/SO_2	0.61	0.96	0.30	
31/03/2017 18:14	CO_2/SO_2	10	0.71	H_2S/SO_2	0.70	0.92	1.40	
31/03/2017 18:26	CO_2/SO_2	46	0.75	H_2S/SO_2	0.55	0.67	0.85	
31/03/2017 23:53	CO_2/SO_2	24	0.62	H_2S/SO_2	0.42	0.79	1.02	
09/04/2017 12:24	CO_2/SO_2	18	0.77	H_2S/SO_2	0.46	0.77	1.00	
09/04/2017 18:12	CO_2/SO_2	24	0.62	H_2S/SO_2	0.58	0.92	0.70	
10/04/2017 00:08	CO_2/SO_2	48	0.82	H_2S/SO_2	0.51	0.75	0.50	
11/04/2017 00:02	CO_2/SO_2	19	0.62	H_2S/SO_2	0.59	0.92	0.80	
11/04/2017 12:21	CO_2/SO_2	16	0.75	H_2S/SO_2	0.52	0.86	0.90	
11/04/2017 18:10	CO_2/SO_2	16	0.69	H_2S/SO_2	0.68	0.99	0.70	
11/04/2017 18:13	CO_2/SO_2	8	0.64	H_2S/SO_2	0.39	0.75	1.00	
11/04/2017 18:15	CO_2/SO_2	23	0.80	H_2S/SO_2	0.60	0.92	0.92	
11/04/2017 18:23	CO_2/SO_2	15	0.89	H_2S/SO_2	0.62	0.83	0.93	PRE-EXPL
12/04/2017 17:53	CO_2/SO_2	85	0.91	H_2S/SO_2	0.03	0.92	12.34	7
12/04/2017 18:15	CO_2/SO_2	20	0.70	H_2S/SO_2	0.46	0.88	0.93	
13/04/2017 00:20	CO_2/SO_2	20	0.80	H_2S/SO_2	0.49	0.91	0.90	
13/04/2017 06:18	CO_2/SO_2	28	0.61	H_2S/SO_2	0.45	0.73	1.10	
13/04/2017 06:25	CO_2/SO_2	33	0.63	H_2S/SO_2	0.46	0.48	0.80	
13/04/2017 12:16	CO_2/SO_2	52	0.67	H_2S/SO_2	0.60	0.94	0.70	

(Continued)

TABLE 2 | Continued

Time	Ratio	Ratio value	R^2	Ratio	Ratio value	R^2	SO_2max (ppmv)	Eruption number
13/04/2017 18:01	CO_2/SO_2	35	0.67	H_2S/SO_2	0.54	0.86	0.68	
14/04/2017 00:09	CO_2/SO_2	14	0.69	H_2S/SO_2	0.03	0.79	0.80	
14/04/2017 00:11	CO_2/SO_2	26	0.66	H_2S/SO_2	0.39	0.88	0.80	
14/04/2017 00:19	CO_2/SO_2	124	0.94	H_2S/SO_2	0.63	0.91	0.91	
18/04/2017 00:19	CO_2/SO_2	32	0.60	H_2S/SO_2	0.52	0.86	0.76	
18/04/2017 12:27	CO_2/SO_2	21	0.60	H_2S/SO_2	0.59	0.78	0.90	
18/04/2017 18:06	CO_2/SO_2	21	0.61	H_2S/SO_2	0.57	0.95	0.70	
18/04/2017 18:11	CO_2/SO_2	17	0.60	H_2S/SO_2	0.69	0.72	0.90	
18/04/2017 18:20	CO_2/SO_2	22	0.86	H_2S/SO_2	0.56	0.90	1.20	
19/04/2017 00:15	CO_2/SO_2	16	0.86	H_2S/SO_2	0.31	0.57	1.17	
19/04/2017 05:58	CO_2/SO_2	19	0.67	H_2S/SO_2	0.60	0.82	0.93	
19/04/2017 18:09	CO_2/SO_2	29	0.68	H_2S/SO_2	0.61	0.88	0.40	
19/04/2017 18:24	CO_2/SO_2	12	0.60	H_2S/SO_2	1.06	0.90	0.36	
20/04/2017 00:01	CO_2/SO_2	118	0.76	H_2S/SO_2	0.53	0.88	0.44	
20/04/2017 00:01	CO_2/SO_2	628		H_2S/SO_2	0.70	0.74	0.75	PRE-EXPL
20/04/2017 00:05	CO_2/SO_2	390	0.98	H_2S/SO_2	0.014	0.95	6.00	8
20/04/2017 06:02	CO_2/SO_2	15	0.71	H_2S/SO_2	0.71	0.90	0.76	
20/04/2017 06:19	CO_2/SO_2	71	0.71	H_2S/SO_2	0.74	0.87	1.00	
20/04/2017 12:11	CO_2/SO_2	34	0.71	H_2S/SO_2	0.49	0.74	0.60	
20/04/2017 23:55	CO_2/SO_2	51	0.76	H_2S/SO_2	0.49	0.95	0.60	
23/04/2017 18:02	CO_2/SO_2	34	0.75	H_2S/SO_2	0.58	0.98	0.40	
24/04/2017 12:11	CO_2/SO_2	13	0.68	H_2S/SO_2	0.54	0.98	0.80	
24/04/2017 12:23	CO_2/SO_2	19	0.72	H_2S/SO_2	0.56	0.89	1.20	
24/04/2017 17:58	CO_2/SO_2	19	0.81	H_2S/SO_2	0.53	0.89	1.20	
24/04/2017 18:17	CO_2/SO_2	43	0.69	H_2S/SO_2	0.62	0.91	0.61	
25/04/2017 00:21	CO_2/SO_2	17	0.89	H_2S/SO_2	0.25	0.60	1.50	
25/04/2017 06:01	CO_2/SO_2	53	0.65	H_2S/SO_2	0.12	0.74	0.85	
25/04/2017 06:02	CO_2/SO_2	241	0.81	H_2S/SO_2	0.44	0.90	0.84	
25/04/2017 06:08	CO_2/SO_2	119	0.64	H_2S/SO_2	0.01	0.99	1.15	
25/04/2017 06:15	CO_2/SO_2	638 (489)	0.71	H_2S/SO_2	0.54 (0.38)	0.99	1.13	PRE-EXPL
25/04/2017 06:21	CO_2/SO_2	55	0.77	H_2S/SO_2	0.004	0.99	34.42	9
25/04/2017 18:11	CO_2/SO_2	28	0.60	H_2S/SO_2	0.67	0.96	1.40	
25/04/2017 18:19	CO_2/SO_2	74	0.95	H_2S/SO_2	0.50	0.95	7.62	
26/04/2017 00:10	CO_2/SO_2	19	0.77	H_2S/SO_2	0.55	0.96	1.01	
26/04/2017 00:27	CO_2/SO_2	16	0.67	H_2S/SO_2	0.65	0.93	1.20	
27/04/2017 00:01	CO_2/SO_2	21	0.66	H_2S/SO_2	0.60	0.93	0.77	
27/04/2017 06:07	CO_2/SO_2	49	0.94	H_2S/SO_2	0.47	0.77	0.30	
28/04/2017 18:13	CO_2/SO_2	16	0.62	H_2S/SO_2	0.33	0.76	0.70	
29/04/2017 00:21	CO_2/SO_2	106	0.67	H_2S/SO_2	0.49	0.98	0.40	
29/04/2017 00:08	CO_2/SO_2	38	0.63	H_2S/SO_2	0.52	0.89	1.20	
29/04/2017 12:25	CO_2/SO_2	7	0.65	H_2S/SO_2	0.41	0.88	1.30	
29/04/2017 18:00	CO_2/SO_2	17	0.90	H_2S/SO_2	0.41	0.73	1.42	
29/04/2017 18:20	CO_2/SO_2	35	0.62	H_2S/SO_2	0.48	0.89	1.34	
30/04/2017 00:10	CO_2/SO_2	35	0.84	H_2S/SO_2	0.69	0.96	0.80	
30/04/2017 18:14	CO_2/SO_2	45	0.70	H_2S/SO_2	0.57	0.81	1.20	
30/04/2017 18:00	CO_2/SO_2	27	0.65	H_2S/SO_2	0.43	0.82	1.18	
30/04/2017 18:19	CO_2/SO_2	39	0.63	H_2S/SO_2	0.50	0.92	1.20	
01/05/2017 12:06	CO_2/SO_2	54	0.68	H_2S/SO_2	0.16	0.38	1.20	
01/05/2017 17:55	CO_2/SO_2	40	0.70	H_2S/SO_2	0.52	0.92	1.26	
01/05/2017 18:10	CO_2/SO_2	51	0.90	H_2S/SO_2	0.55	0.97	1.08	

(Continued)

TABLE 2 | Continued

Time	Ratio	Ratio value	R^2	Ratio	Ratio value	R^2	SO_2max (ppmv)	Eruption number
02/05/2017 00:04	CO_2/SO_2	10	0.75	H_2S/SO_2	0.50	0.99	1.20	
02/05/2017 00:09	CO_2/SO_2	16	0.77	H_2S/SO_2	0.55	0.99	0.91	
02/05/2017 00:21	CO_2/SO_2	27	0.82	H_2S/SO_2	0.58	0.92	1.25	
02/05/2017 12:10	CO_2/SO_2	35	0.74	H_2S/SO_2	0.43	0.88	1.01	
02/05/2017 12:25	CO_2/SO_2	63	0.81	H_2S/SO_2	0.42	0.95	1.10	
02/05/2017 18:14	CO_2/SO_2	56	0.84	H_2S/SO_2	0.29	0.78	1.00	
03/05/2017 00:05	CO_2/SO_2	56	0.82	H_2S/SO_2	0.33	0.92	0.80	
03/05/2017 00:13	CO_2/SO_2	54	0.84	H_2S/SO_2	0.50	0.88	0.92	
03/05/2017 00:22	CO_2/SO_2	34	0.82	H_2S/SO_2	0.44	0.96	1.09	
03/05/2017 06:01	CO_2/SO_2	50	0.67	H_2S/SO_2	0.37	0.86	0.80	
03/05/2017 06:05	CO_2/SO_2	60	0.64	H_2S/SO_2	0.37	0.89	0.75	
03/05/2017 06:10	CO_2/SO_2	56	0.70	H_2S/SO_2	0.43	0.82	0.68	
03/05/2017 06:18	CO_2/SO_2	72	0.63	H_2S/SO_2	0.34	0.79	0.76	
04/05/2017 00:00	CO_2/SO_2	26	0.65	H_2S/SO_2	0.42	0.86	0.70	
04/05/2017 00:15	CO_2/SO_2	37	0.82	H_2S/SO_2	0.64	0.93	0.77	
04/05/2017 06:09	CO_2/SO_2	22	0.67	H_2S/SO_2	0.42	0.93	1.00	
04/05/2017 06:17	CO_2/SO_2	38	0.63	H_2S/SO_2	0.53	0.91	0.76	
04/05/2017 18:21	CO_2/SO_2	38	0.87	H_2S/SO_2	0.52	0.91	1.10	
04/05/2017 17:57	CO_2/SO_2	19	0.63	H_2S/SO_2	0.46	0.88	1.25	
05/05/2017 00:04	CO_2/SO_2	14	0.60	H_2S/SO_2	0.62	0.89	0.50	
05/05/2017 12:02	CO_2/SO_2	3	0.74	H_2S/SO_2	0.56	0.97	1.20	
05/05/2017 18:26	CO_2/SO_2	4	0.90	H_2S/SO_2	0.52	0.98	1.20	
08/05/2017 00:15	CO_2/SO_2	6	0.80	H_2S/SO_2	0.64	0.97	1.41	
08/05/2017 00:22	CO_2/SO_2	17	0.76	H_2S/SO_2	0.27	0.52	1.01	
08/05/2017 12:07	CO_2/SO_2	68	0.61	H_2S/SO_2	0.35	0.83	0.80	
08/05/2017 12:27	CO_2/SO_2	116	0.62	H_2S/SO_2	0.35	0.71	0.76	
08/05/2017 18:18	CO_2/SO_2	38	0.77	H_2S/SO_2	0.49	0.92	1.26	
08/05/2017 17:57	CO_2/SO_2	127	0.69	H_2S/SO_2	0.54	0.92	0.69	
09/05/2017 00:23	CO_2/SO_2	67	0.65	H_2S/SO_2	0.41	0.81	1.20	
09/05/2017 06:05	CO_2/SO_2	86	0.60	H_2S/SO_2	0.44	0.67	0.40	

*The R^2 values ($\geq$ 0.6 in all cases) identify the regression coefficients in the CO_2 vs. SO_2 and H_2S vs. SO_2 scatter plots that concurred to determine each ratio. SO_2 max identifies the peak SO_2 concentration within each measurement interval. All data refer to quiescent gas except for those associated with an eruption number (which correspond to the syn-explosive gas). The quiescent gas measured prior to each explosion is referred as pre-explosive gas (PRE-EXPL in the table). The quoted compositions for the pre-explosive gas are 20-min averages of point-to-point ratios, e.g., calculated by taking the ratios of individual co-acquired gas concentration couples. Based on laboratory tests, we estimate error in these point-to-point ratios at ~50%, so the quoted values should only be viewed as semi-quantitative estimates. Only in 2 cases (out of 9 explosions), gas mixing rates were correlated to significant levels (R^2 > 0.6) to allow ratios to be derived with the correlation plot methodology also (see **Figures 4a**, **6a**). The scatter plot-derived gas ratios are listed in parenthesis for comparison in the table.*

onset is rapid and abrupt, as indicated by the gas ratio contrast between the *pre-explosive gas* and *explosive gas* (**Figures 4a**, **6a**);

iii) both the *quiescent gas* and *syn-explosive gas* are similarly CO_2-rich (relative to S;) compared to magmatic gases in Costa Rica and Nicaragua (see **Figure 7** and reference therein).

iv) The quiescent gas vented prior to an explosion (the *pre-explosive gas*) has systematically higher CO_2/SO_2 ratios than the corresponding *explosive gas* (**Figures 4**, **6**). This difference can only partially reflect the different data processing technique (point-to-point vs. scatter plot, see **Figures 4**, **6**). Thus, also in view of the H_2S/SO_2 records discussed above (see point ii), we conclude that the *explosive gas* is especially SO_2-rich.

These peculiar features of the Rincón de la Vieja crater lake plume have implications for the nature of the magmatic-hydrothermal system producing the emissions, and for the trigger mechanisms of the recurrent explosions, as detailed below.

Rincon de la Vieja Gas Signature: Magmatic or Hydrothermal?

In contrast to the less active (e.g., less acidic) volcanic lakes fed by hydrothermal H_2S only (e.g., Hasselle et al., 2018), the low (typically <1) H_2S/SO_2 ratios in the Rincón de la Vieja crater lake gas suggest supply of oxidized (SO_2-dominated) magmatic fluids into the lake system (Christenson et al., 2010; Christenson and Tassi, 2015). Magmatic gases typically display equilibrium H_2S/SO_2 ratios buffered by redox conditions in the coexisting

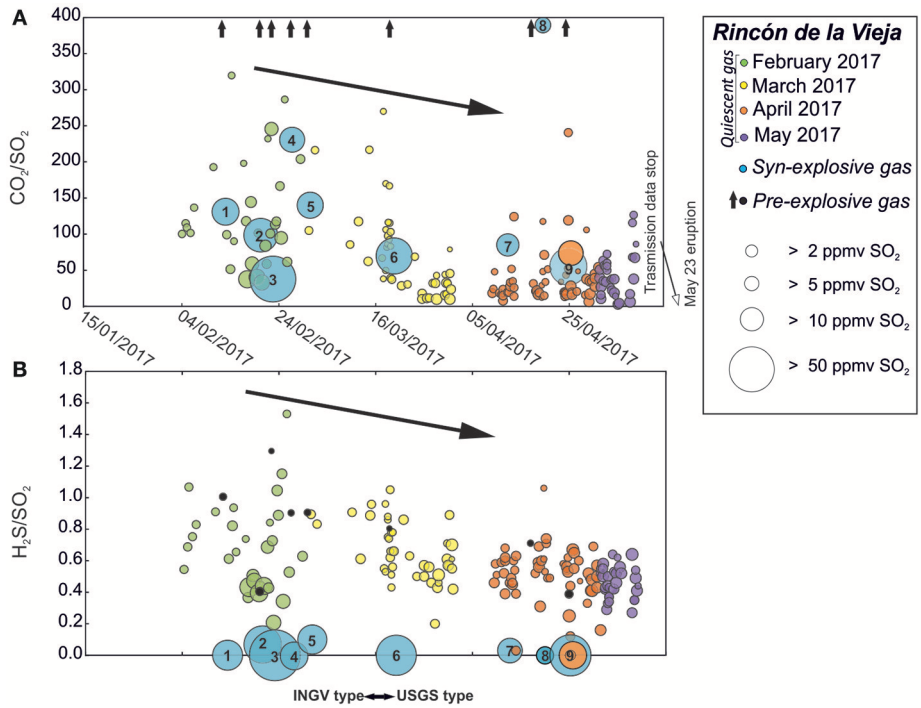

FIGURE 5 | Time-series of gas **(A)** CO_2/SO_2 and **(B)** H_2S/SO_2 (molar) ratios. *Quiescent gases, pre-explosive gases* and *syn-explosive gases* are plotted with different colors. Symbol size is proportional to SO_2 mixing ratios. In **(A)**, all *pre-explosive gases* plot at higher CO_2/SO_2 ratios (as shown by the arrows).

silicate melt, according to Giggenbach (1987):

$$SO_2 + 3H_2 = H_2S + 2H_2O \quad (2)$$

This magma-inherited H_2S/SO_2 ratio is then generally preserved during rapid ascent and cooling of magmatic gases, unless hydrothermal storage and re-equilibration occurs (Giggenbach, 1987). Resolving Equation (2) over a range of magmatic temperatures, and at redox conditions (e.g., H_2/H_2O ratios) buffered by the silicate melt at QFM (quartz-fayalite-magnetite) and NNO (Nickel-Nickel oxide) buffers (Carmichael and Ghiorso, 1986), a range of equilibrium H_2S/SO_2 ratios can be obtained (as illustrated in **Figure 8**), well encompassing the Rincón de la Vieja crater lake gas range. For example, gases separating from magma at ∼900°C and QFM will have equilibrium H_2S/SO_2 of ∼1 (constituting the so-called magmatic gas H_2S/SO_2 buffer of Giggenbach, 1987), similar to gases from the Rincón de la Vieja crater lake (**Figures 7**, **8**).

A continuous supply of SO_2-rich magmatic gases to the lake is also consistent with the dissolved ion composition of the crater lake water, placing Rincón de la Vieja in the field of high-activity volcanic lakes according to the classification of Pasternack and Varekamp (1997) and Varekamp et al. (2000). Tassi et al. (2005, 2009) argue that the high Cl^-/Na^+ ratio in the Rincón de la Vieja crater lake requires supply of magmatic HCl into the lake, a process also responsible for the high SO_4^{2-} and F^- concentrations (from the dissolution of magmatic SO_2, H_2S, and HF). The hyper-acidic chloride–sulfate brine filling the crater lake is also rich in aluminum, iron, zinc, copper, and boron (because of elemental input via both magmatic gases and enhanced rock dissolution), and is thus compositionally similar to the magmatic gas-fed Laguna Caliente Crater Lake, Poás volcano (Tassi et al., 2009).

Whereas, S speciation and lake chemistry clearly support magmatic gas feeding the lake, the high CO_2/SO_2 signature of the Rincón de la Vieja crater lake gas is inconsistent with a "pure magmatic" hypothesis. **Figure 7** compares the Rincón de la Vieja gas compositions (this work and previous studies) with gases emitted by other recently active Costa Rican volcanoes (Poás and Turrialba; de Moor et al., 2016a,b, 2017). Both Poás and Turrialba datasets show a spread of volcanic gas compositions, which have been interpreted as reflecting variable extents of mixing between magmatic and hydrothermal end-members (Fischer et al., 2015; de Moor et al., 2016a,b). The magmatic CO_2/SO_2 end-members (see stars in **Figure 7**) have been estimated at ∼0.3–0.5 (Poás) and ∼1–2 (Turrialba), well below the Rincón de la Vieja crater lake gas range for both quiescent and syn-explosive gas types. Similarly, gas observations at nearby Nicaraguan volcanoes Masaya and Momotombo imply a magmatic gas CO_2/SO_2 ratio of ∼3–6 (Aiuppa et al., 2014, 2017; de Moor et al., 2017), again implying that the Rincón de la Vieja crater lake gas in 2017 has too high CO_2/SO_2 to be interpreted as pure magmatic (see **Figure 7**).

The CO_2-rich composition of Rincón de la Vieja crater lake gases also does not agree with magmatic degassing models (Moretti et al., 2003) using input conditions relevant to Costa Rica-like magma (see de Moor et al., 2016b for details).

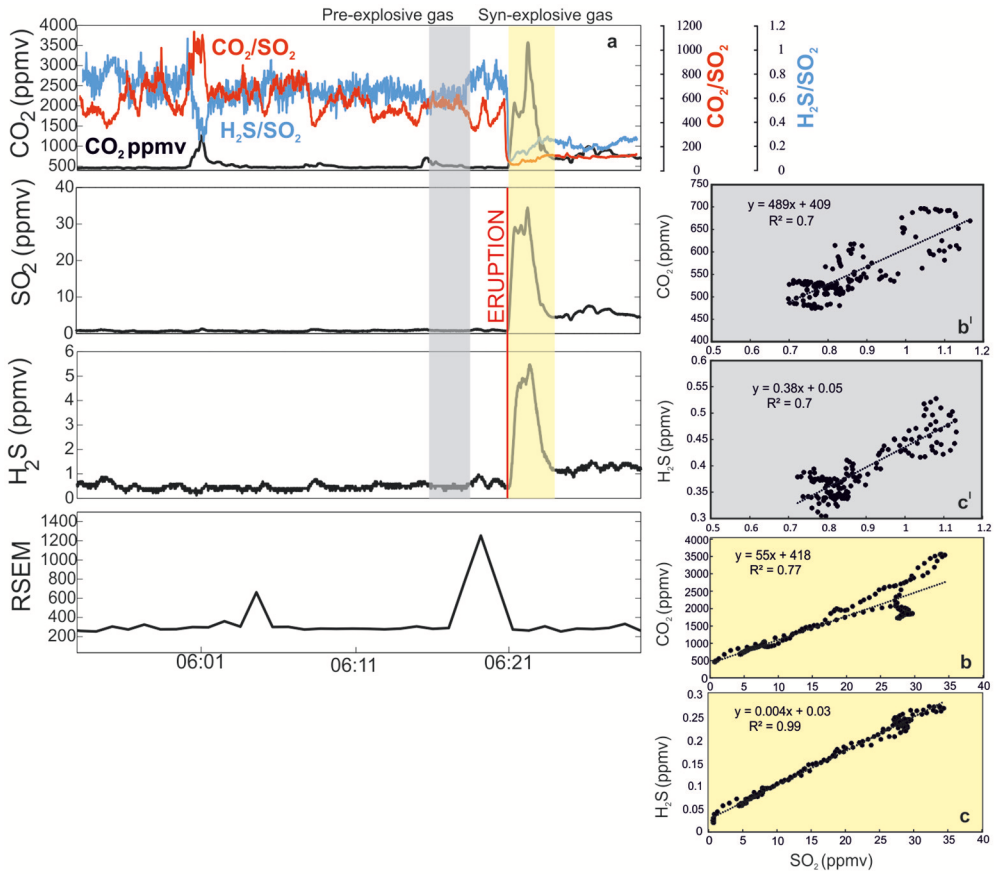

FIGURE 6 | (a) Detail of gas and seismic records taken on April 25, 2017 between ~5:51 and ~6:31 GMT. The eruption (event #9 in **Figure 3**, see inset) occurred at ~6.21 GMT. Mixing ratios increase after the blast. The yellow-colored area corresponds to the sub-interval (identified with Ratiocalc) where CO_2, SO_2, and H_2S are positively correlated at statistically significant level ($R^2 > 0.6$). These subsets of CO_2, SO_2, and H_2S mixing ratios are used to draw **(b)** CO_2 vs. SO_2 and **(c)** H_2S vs. SO_2 correlation plots, and to calculate the time-averaged CO_2/SO_2 and H_2S/SO_2 ratios (within the yellow-colored temporal windows) from the slopes of the best-fit regression lines (listed in **Table 2**). In **(a)** the red and blue lines are high-resolution (1 Hz) records of CO_2/SO_2 and H_2S/SO_2 ratios, respectively, calculated by taking the ratio of individual couples of co-acquired mixing ratios. This point-to-point ratios suggest contrasting gas signatures for *pre-explosive* and *syn-explosive gas*. Example of CO_2 vs. SO_2 and H_2S vs. SO_2 correlation plots for the *pre-explosive gas* [built from data within the gray-colored temporal windows in **(a)**], shown in **(b')** and **(c')**.

These numerical simulations (see **Figure 7**) predict equilibrium CO_2/SO_2 ratios of 20 to 0.07 for gases exsolved from a Turrialba-like andesitic magma (at redox condition of QFM +1 to +3 and temperatures of 900–1,100°C) decompressed from 250 MPa to 0.1 MPa pressure. The measured CO_2/SO_2 ratios in Rincón de la Vieja crater lake gas (64±59 and 136±110 for the *quiescent* and *syn-explosive gas*, respectively) are clearly higher than the typical magmatic range, unless very high gas-melt separation pressures (>> 250 MPa, equivalent to > 9 km depth) are assumed. Such a deep magma source is unlikely, however, because heat pipes typically sustaining intense degassing and convective overturning at crater lakes require shallow magma (**Figure 9**; Christenson and Tassi, 2015). Also, magma involvement in the recent Rincón de la Vieja eruptions (implicated by the small but ubiquitous juvenile fragments in the eruption deposits) is indicative of shallow storage (**Figure 9**).

To summarize, the CO_2-rich gas compositions with low H_2S/SO_2 ratios (**Figure 7**) are incompatible with a direct shallow magmatic source for the gas vented by the Rincón de la Vieja crater lake. We propose that the pristine chemical composition of deep magmatic gases is altered during upward migration by gas-water-rock reactions within the (sub)limnic hydrothermal system.

The Role of the Sublimnic Hydrothermal System

The interactions of magmatic gases with either the crater lake or the subjacent hydrothermal system are the most obvious candidates for generating the observed CO_2-rich (S-depleted) Rincón de la Vieja gas. Magmatic gas-lake and/or magmatic-hydrothermal reactions, if occurring, could also effectively control S partitioning between reduced and oxidized forms, thus modifying the original magmatic H_2S/SO_2 ratio (Christenson et al., 2010; Christenson and Tassi, 2015).

One often-invoked mechanism of magmatic SO_2 dissolution into active volcanic lakes is via disproportionation reactions such

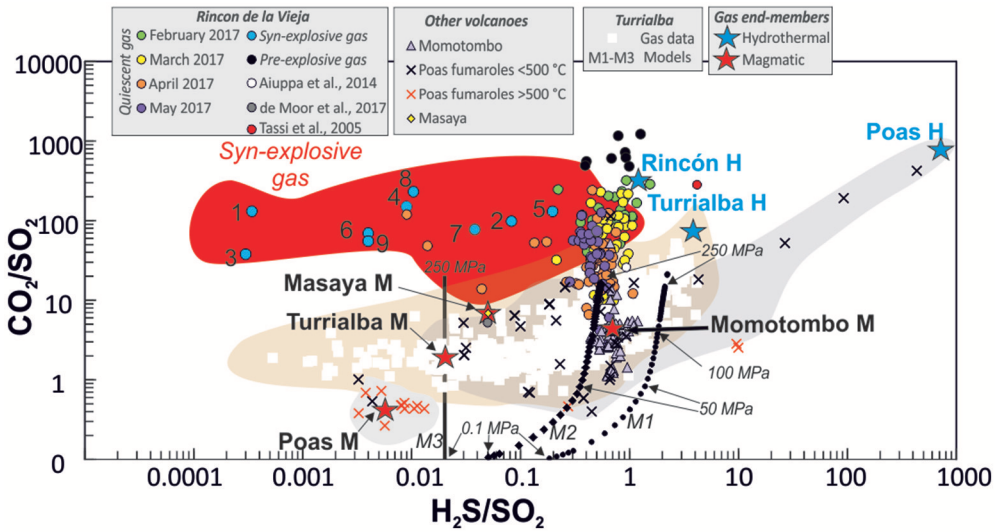

FIGURE 7 | H_2S/SO_2 vs.CO_2/SO_2 scatter plot of Costa Rica and Nicaraguan volcanic gases. The Rincón de la Vieja gas (both *quiescent gas* and *syn-explosive gas*; same symbols as in **Figure 5**) is contrasted with the composition of volcanic gases from other volcanoes of the Costa Rica-Nicaragua arc segment. Momotombo and Masaya: (Aiuppa et al., 2014, 2017; de Moor et al., 2017); Poas: (Aiuppa et al., 2017; de Moor et al., 2017). Estimated compositional fields for hydrothermal (H) and magmatic (M) end-members are indicated (this study; based on averaging of magmatic and hydrothermal compositions quoted in the previous studies). The hypothetical composition of the Rincón hydrothermal pole (H) was estimated by averaging composition of the two measurements of *quiescent gases* with the lowest SO_2 concentrations (e.g., the most hydrothermal endmember). Numbers alongside the *syn-explosive gas* data-points identify the explosions (see **Figure 3**). The curves labeled M1 to M3 indicate the model-derived H_2S/SO_2 vs.CO_2/SO_2 compositions obtained by model simulations of degassing upon decompression (from 250 to 0.1 MPa) for a Turrialba-like magma (taken from de Moor et al., 2016b). M1 and M2 models have been initialized at slightly different H_2O contents (3 and 2 wt. %, respectively). In model M3, gas compositions obtained in runs M1-M2 are re-calculated at surface discharge conditions (QFM+3, 0.1 MPa, 650°C), yielding H_2S/SO_2 ratio of ∼0.02 (see the original work of de Moor et al., 2016b for further details).

as (Kusakabe et al., 2000):

$$3SO_2 + 2H_2O \rightarrow 2HSO_{4^-} + S_{(e)} + 2H^+ \quad (3a)$$

$$4SO_2 + 4H_2O \rightarrow 3HSO_{4^-} + H_2S + 3H^+ \quad (3b)$$

The two relationships can be combined into the following equilibrium:

$$SO_2 + S_{(e)} + 2H_2O = H_2S + H^+ + HSO_{4^-} \quad (4)$$

To assess the role played by magmatic gas-lake water reactions, we test if the measured H_2S/SO_2 ratios in the Rincón de la Vieja gas (**Figures 4**–**8**) are consistent with the equilibrium ratio predicted by Equation (4) at lake water conditions, i.e., if the measured gas S speciation is controlled/buffered by dissolved S species in the crater lake water. In the Rincón de la Vieja crater lake, oxidized (exavalent) dissolved S species prevail (Tassi et al., 2005), and sulfur spherules are always observed on the lake surface (**Figure 2**), implying that all of the ingredients for reaction 4 are available in abundance. Solving Equation (4) for the H_2S/SO_2 gas ratio, at crater lake water conditions (T = 30–50°C; $H_2SO_4 = 8.16 \times 10^{-12}$ M at pH = 0.77 and $SO_4^{2-} = 0.146$ M), and using the thermodynamic data from HSC thermochemical software (http://www.hsc-chemistry.com/), we obtain the curve labeled "*Lake*" in **Figure 8**. The H_2S/SO_2 gas ratios predicted by reaction (4) are, however, H_2S-dominated, pointing against a lake-buffered H_2S/SO_2 ratio hypothesis (**Figure 8**). Our calculations thus suggest that either a kinetic process prevails (e.g., that Equation 4 does not go to completion in the lake, leading to only partial conversion of magmatic SO_2 into H_2S) (Ohmoto and Lasaga, 1982; Rye, 2005), or that magmatic gas-water interactions occur deeper in the system, such as in the hotter sublimnic hydrothermal system (**Figure 9**).

A variety of magmatic gas-water-rock reactions have been proposed to occur in sublimnic hydrothermal systems (Christenson and Tassi, 2015; Shinohara et al., 2015). These hydrothermal reactions, typically occurring in the upper portion of a heat pipe (**Figure 9**), invariably enrich the gas phase in CO_2 relative to more reactive SO_2 and H_2S (Symonds et al., 2001, 2003), and may thus generate the high CO_2/SO_2 ratios in Rincón de la Vieja crater lake gas. In addition to leading to S depletion, these reactions can also act as controls on the H_2S/SO_2 ratio (see below).

In addition to the reaction described by Equation (4), S scrubbing can occur via (Giggenbach, 1987; Christenson and Tassi, 2015):

$$2H_2S_{(g)} + SO_{2(g)} = 3S_{(e)} + 2H_2O \quad (5)$$

This reaction scavenges H_2S and SO_2 in 2:1 proportions, and can thus (at least partially) justify the oxidized nature ($SO_2 > H_2S$) of the Rincón de la Vieja gas. In fact, the situation is more complicated, because as pointed out by Shinohara et al. (2011), S deposition via Equation (5) can either increase or decrease

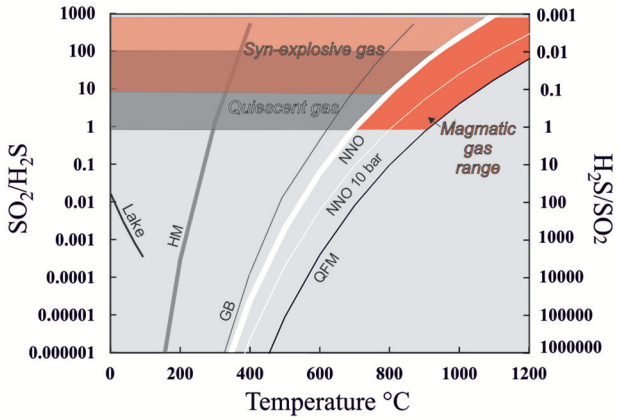

FIGURE 8 | Temperature dependence of the SO_2/H_2S ratio, as predicted by the common magmatic and hydrothermal redox buffers (modified from Aiuppa et al., 2005). The solid lines represent the H_2S/SO_2 ratios at equilibrium with redox conditions (oxygen fugacity, fO_2) fixed by QFM (Quartz-Fayalite-Magnetite), NNO (Nickel-Nickel oxide), and HM (Hematite-magnetite) redox buffers (Giggenbach, 1987, 1996). The magmatic gas range is from Aiuppa et al. (2005). The curve labeled GB and Lake illustrate the equilibrium H_2S/SO_2 ratios at redox conditions fixed by the Giggenbach (1987) FeO-$FeO_{1.5}$ hydrothermal buffer (Equation 6) and dissolved S species in the lake buffer water (Equation 2), respectively. Pressure is 1 bar except where specified. The measured H_2S/SO_2 ranges for both the *quiescent* and *syn-explosive* gas are indicated by gray and red bands, respectively.

the gas H_2S/SO_2 ratio, depending on the original S speciation (SO_2-dominated or H_2S-dominated) in the feeding magmatic gas entering the hydrothermal system (unconstrained for Rincón). Also, concurrently with hydrothermal S deposition, iron minerals in the hydrothermal rock matrix can contribute buffering redox conditions (e.g., the gas H_2/H_2O ratio), via (Giggenbach, 1987):

$$4FeO_{1.5} + 2H_2 = 4(FeO) + 2H_2O \quad (6)$$

$$4Fe_3O_4 + 2H_2O = 6Fe_2O_3 + 2H_2 \quad (7)$$

These reactions can then buffer, via Equation (2), the residual (after S deposition) hydrothermal gas H_2S/SO_2 ratio. For example, the H_2S/SO_2 gas ratios predicted (as a function of temperature) from Equation (2), and redox conditions buffered by either the Fe(II)-Fe(III) hydrothermal buffer (Equation 6; Giggenbach, 1987) or the Hematite-Magnetite buffer (HM) hydrothermal (Equation 7), are graphically illustrated in **Figure 8**. The figure shows that the measured H_2S/SO_2 ratios in the Rincón de la Vieja gas would be consistent with those imposed by hydrothermal buffering at HM redox conditions, 290–400°C, and 1 bar (**Figure 8**). Coexistence of oxidized (hematite) and reduced (magnetite, pyrite) iron forms is suggested at both Rincón de la Vieja (Tassi et al., 2005) and in the nearby Borinquen and Miravalles hydrothermal fields (Gherardi et al., 2002; Molina and Martí, 2016). However, since a second independent redox couple (e.g., the H_2/H_2O ratio; Aiuppa et al., 2011) is not measured in the Rincón gas, evidence for hydrothermal (HM) buffering of S speciation remains speculative.

In summary, available gas information at Rincón de la Vieja is suggestive of extensive hydrothermal processing of magmatic gases within the sublimnic hydrothermal system. These hydrothermal reactions consume S (compared to relatively inert C, thus explaining the high observed CO_2/S ratio), but the exact S deposition mechanisms (Equations 3–5), and perhaps the role of hydrothermal redox buffering (Equation 7), cannot be quantitatively constrained with the present data. However the observed difference in H_2S/SO_2 between the *quiescent gas* (0.57 ± 0.20) and the *syn-explosive gas* (0.04 ± 0.06), and the abrupt gas ratio changes at eruption onsets (**Figures 4a**, **6a**), clearly imply less hydrothermal interaction (e.g., less SO_2 deposition) during the phreatic blasts (**Figure 9**). This can be explained by a combination of faster gas transit, transient disruption of the sublimnic hydrothermal envelop, and/or deeper (hotter) gas source during the explosions (**Figure 9**).

The Eruption Trigger

Whatever the exact process (Equations 3–6), S scrubbing reactions are likely to lead to rapid and effective formation of native S seals (Christenson and Tassi, 2015). The presence of S spherules in the Rincón de la Vieja crater lake points to the existence of a native sulfur layer at the lake bottom (Hurst et al., 1991; Takano et al., 1994; Christenson et al., 2010) (**Figure 9**).

The physical state of this S pool is known to be dependent on temperature, with a ∼2000-times viscosity increase upon heating in the 150–200°C temperature range (Hurst et al., 1991; Oppenheimer, 1992; Takano et al., 1994). It is possible that magmatic-hydrothermal gases, while persistently fluxing through the Rincón de la Vieja sublimnic hydrothermal system, progressively heat the S pool, thus ultimately creating the conditions for the development of a viscous impermeable seal (**Figure 9A**).

We envision a mechanism in which, during quiescence (**Figure 9A**), the feeding magmatic gas interacts with the sublimnic hydrothermal system, undergoes S deposition (± buffering by hydrothermal minerals) and develops a CO_2-rich gas. A fraction of this gas, perhaps after further S deposition into the lake, is emitted to the surface as *quiescent gas*, but the remaining fraction is accumulated at depth as the impermeable S seal develops (**Figure 8a**). The *quiescent gas* released shortly prior to explosions, e.g., the *pre-explosive gas*, is characterized by low gas mixing ratios and especially high CO_2/SO_2 ratios, consistent with a reduction of gas transfer from underneath the seal, and extensive S loss to hydrothermal minerals (**Figures 4a**, **6a**).

Ultimately, gas accumulation underneath the seal leads to pressure buildup and seal failure to trigger a phreatic explosion (**Figure 9B**). This mechanism is also supported by the recurrent observation in the erupted products, especially in the 1–2 mm ash grain-size fraction, of native sulfur fragments. We argue that, during the phreatic blasts, rapid gas ascent reduces hydrothermal interactions as supported by the observed short-term variations in gas chemistry. In fact, our high-resolution (1 Hz) of CO_2/SO_2 and H_2S/SO_2 records (see **Figures 4a**, **6a**) show that both ratios suddenly decrease at the eruption onset, implying the each *syn-eruptive gas* is SO_2-richer than its corresponding *pre-explosive gas*. Rapid gas ascent, perhaps combined with gas ascent from

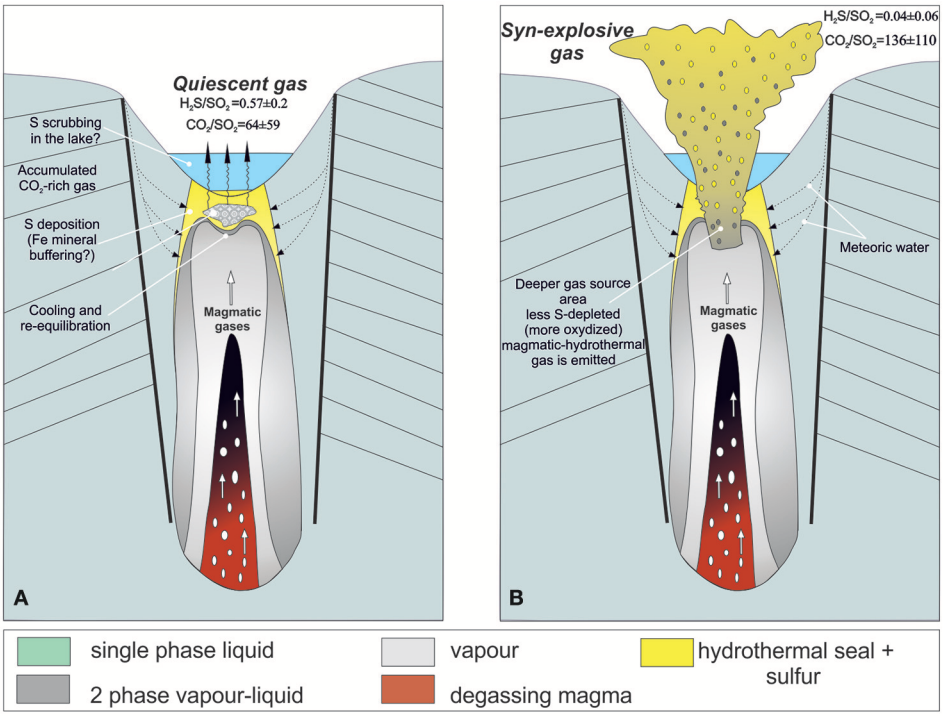

FIGURE 9 | A schematic model for the Rincón de la Vieja volcano shallow feeding system, detailing the structure of the sublimnic hydrothermal/magmatic system (modified from Christenson et al., 2010). **(A)** During quiescence, the feeding magmatic gas undergoes S deposition (± buffering by hydrothermal minerals) within the sublimnic hydrothermal system. The resulting CO_2-rich gas is partially surface-vented as *quiescent gas*, and partially accumulated beneath an impermeable S seal; **(B)** pressure buildup below the S seal triggers a phreatic explosion, characterized by rapid gas ascent, limited hydrothermal interaction, and deeper gas source. This *syn-explosive gas* retains a C-rich signature, implying a magmatic-hydrothermal nature.

deeper/hotter portions of the magmatic-hydrothermal vapor zone (**Figure 9B**), are likely implicated in producing the relatively SO_2-richer *syn-explosive gas*.

We caution that our interpretation is based on only ∼3 months of observations and the capturing of only 9 out of 42 explosions in that time interval. Thus, longer observations are required to draw more concrete conclusions. However, our results confirm that continuous instrumental geochemical monitoring, in tandem with seismic monitoring, can contribute to understanding the mechanisms that drive the Rincón de la Vieja magmatic system toward potentially hazardous critical states. It is interesting to note that both the H_2S/SO_2 and CO_2/SO_2 ratios in the Rincón de la Vieja *quiescent gas* decreased from February to early May (**Figures 5**, **7**), implying a decreasing extent of hydrothermal re-equilibration of the feeding magmatic gases. This trend toward more magmatic-like gas composition may tentatively be interpreted as reflecting an increase in the magmatic gas supply to the lake conduit, and thus a more unstable magmatic system leading to the major lahar-generating phreatic eruption of May 23 (Global Volcanism Program, 2017), which occurred just a few weeks after our Multi-GAS dataset ended (and actually destroyed the instrument). As stated above, this event (and the following June 11 event) erupted a sizeable juvenile fragment component, claiming for escalating magmatic activity.

Implications for Monitoring of Active Crater Lakes

Our measurements of the syn-explosive gas, the first of their nature at an active volcano, provide observational evidence for that formation of hydrothermal S seals may strongly be implicated in the generation of phreatic eruptions, as originally proposed at Ruapehu volcano in New Zeeland (Hurst et al., 1991; Takano et al., 1994; Christenson et al., 2010). It is arguable that hydrothermal seal formation may fuel phreatic/phreatomagmatic activity at other recurrently erupting volcanic lakes worldwide (Christenson and Tassi, 2015; Stix and de Moor, 2018). As our Rincón de la Vieja dataset shows, continuous gas records may help tracking such seal formation events, as marked by phases of reduced surface S degassing (see the low SO_2 and H_2S mixing ratios, and high CO_2/SO_2 ratios, in the *pre-explosive gas*; **Figures 4a**, **6a**, **7**). To test this hypothesis further, our results thus claim for the need of augmenting the number of volcanic crater lakes that are monitored by permanent gas instrumentation.

It is also interesting to note that the rapid and abrupt transition between *pre-explosive* and *explosive gas* at Rincón de la Vieja (**Figures 4a**, **6a**), pointing to reduced surface S outgassing prior to each blast, is in stark contrast with what recurrently reported at Poás, where precursory trends toward more magmatic (more S-rich) gas composition are observed

instead (de Moor et al., 2016a). We argue this difference may imply an overall lower magmatic gas input, or a more effective seal (or both), at Rincón de la Vieja, compared to the more active Poás volcano (where the magmatic system appears more implicated as eruption trigger). This comparison suggests that distinct trigger mechanisms, with different relative roles played by hydrothermal sealing vs. magmatic as influx, may in fact be operating at active crater lakes. This diversity in potential trigger mechanisms (Stix and de Moor, 2018) reinforces the need for more robust (and temporally continuous) gas records at volcanic crater lakes.

CONCLUSIONS

This study investigates degassing dynamics of Rincón de la Vieja during a period of intense phreatic activity. For the first time at any volcano, the composition of the gas released during discrete phreatic events (confirmed seismically) was resolved using Multi-GAS. Our results demonstrate chemically distinct gas compositions during quiescent degassing vs. explosive eruptive degassing. The *quiescent* gas is characterized by very low concentrations of sulfur gas species (SO_2 and $H_2S < 2$ ppmv) and relatively high H_2S/SO_2 ratios (mean 0.57), whereas the *syn-explosive* gas shows much higher gas mixing ratios of SO_2 and CO_2 and a systematic decrease of H_2S/SO_2 ratio (mean, 0.04). Both the *quiescent* and *syn-explosive* gases exhibit high CO_2/S ratios relative to regional magmatic gases, but each *explosive gas* has lower CO_2/S ratio than its corresponding *pre-explosive gas*.

These C-rich gases, if interpreted as magmatic, would require a very deep ($P > 250$ MPa) magmatic source, which is unlikely in view of the recent magma involvement in the 2017 Rincón phreatomagmatic eruptions. We thus favor a mechanism in which magmatic gas-water-rock reactions in the sublimnic hydrothermal system lead to deposition of native S and sulfate formation, and thus enrich the gas phase in C relative to SO_2 and H_2S. The presence of abundant native sulfur spherules in the lake is consistent with this scenario, as the presence of S spherules suggests a native sulfur layer at the lake bottom. We propose that continuous gas fluxing may progressively lead to development of an impermeable seal near the lake/hydrothermal system interface. Gas accumulates underneath the seal, and ultimately ruptures this seal resulting in phreatic eruptions. The trend of decreasing *quiescent* CO_2/SO_2 and H_2S/SO_2 ratios from February to May 2017 can be interpreted as an increase in the magmatic gas supply, providing a precursor to the major eruption of 23 May.

These results, the first volcano reports for the gas phase released by discrete phreatic eruptions, confirm (Christenson and Tassi, 2015) that the complex interplay between rising magmatic gases and the sublimnic hydrothermal system likely plays a decisive role in triggering the explosions.

DATA AVAILABILITY STATEMENT

The raw data supporting the conclusions of this manuscript will be made available by the authors, without undue reservation, to any qualified researcher.

AUTHOR CONTRIBUTIONS

AB, JMdM, and AA conceived the idea. AB, JMdM, GA, HB, HV, MB, GG, and PK prepared the instrumentation and conducted the field experiment. AB, MM, HB, and DD processed the data. AB and AA drafted the article with help from JMdM, PK, GA, HB, and MM.

ACKNOWLEDGMENTS

We wish to thank Franco Tassi, Orlando Vaselli, Giulio Bini, and ICE staff for help during Multi-GAS installation. We gratefully acknowledge OVSICORI for logistical support. We also thank Bill Evans (USGS), Ryunosuke Kazahaya, Hiroshi Shinohara, Paul Wallace, and Jacob Lowenstern, whose thoughtful comments improved the quality of this work. This research has been funded by the Deep Carbon Observatory via the DECADE research initiative (Grant no. 10759-1238, AA). JMdM gratefully acknowledges support through the Deep Carbon Observatory's Biology Meets Subduction project. Any use of trade, firm, or product names is for descriptive purposes only and does not imply endorsement by the U.S. Government.

REFERENCES

Aiuppa, A. (2015). "Volcanic-gas monitoring," in *Volcanism and Global Environmental Change*, eds A. Schmidt, K. Fristad, and L. Elkins-Tanton (Cambridge: Cambridge University Press), 81–96. doi: 10.1017/CBO9781107415683.009

Aiuppa, A., Bertagnini, A., Métrich, N., Moretti, R., Di Muro, A., Liuzzo, M., et al. (2010). A model of degassing for Stromboli volcano. *Earth Planet. Sci. Lett.* 295, 195–204. doi: 10.1016/j.epsl.2010.03.040

Aiuppa, A., de Moor, J. M., Arellano, S., Coppola, D., and Francofonte, V., Galle, B., et al. (2018). Tracking formation of a lava lake from ground and space: Masaya volcano (Nicaragua), 2014–2017. *Geochem. Geophys. Geosyst.* 19, 496–515. doi: 10.1002/2017GC007227

Aiuppa, A., Federico, C., Giudice, G., Gurrieri, S., Liuzzo, M., Shinohara, H., et al. (2006), Rates of carbon dioxide plume degassing from Mount Etna volcano. *J. Geophys. Res. Solid Earth* 111, 1–8. doi: 10.1029/2006JB004307

Aiuppa, A., Fischer, T. P., Plank, T., Robidoux, P., and Di Napoli, R. (2017), Along-arc, inter-arc and arc-to-arc variations in volcanic gas CO2/ST ratios reveal dual source of carbon in arc volcanism. *Earth Sci. Rev.* 168, 24–47. doi: 10.1016/j.earscirev.2017.03.005

Aiuppa, A., Inguaggiato, S., McGonigle, A. J. S., O'Dwyer, M., Oppenheimer, C., Padgett, M. J., et al. (2005), H_2S fluxes from Mt. Etna, Stromboli, and Vulcano (Italy) and implications for the sulfur budget at volcanoes. *Geochim. Cosmochim. Acta* 69, 1861–1871. doi: 10.1016/j.gca.2004.09.018

Aiuppa, A., Robidoux, P., Tamburello, G., Conde, V., Galle, B., Avard, G., et al. (2014), Gas measurements from the Costa Rica-Nicaragua volcanic segment suggest possible along-arc variations in volcanic gas chemistry. *Earth Planet. Sci. Lett.* 407, 134–147. doi: 10.1016/j.epsl.2014.09.041

Aiuppa, A., Shinohara, H., Tamburello, G., Giudice, G., Liuzzo, M., and Moretti, R. (2011). Hydrogen in the gas plume of an open-vent volcano, Mount Etna Italy. *J. Geophys. Res. Solid Earth* 116, 1–8. doi: 10.1029/2011JB008461

Alvarado, G. E., Kussmaul, S., Chiesa, S., Gillot, P. Y., Appel, H., Worner, G., et al. (1992). Resumen cronoestratigrafico de las rocas igneas de Costa Rica basado en dataciones radiometricas. *J. South Am. Earth Sci.* 6, 151–168. doi: 10.1016/0895-9811(92)90005-J

Alvarado, G. E., Mele, D., Dellino, P., de Moor, J. M., and Avard, G. (2016). Are the ashes from the latest eruptions (2010–2016) at Turrialba volcano (Costa Rica) related to phreatic or phreatomagmatic events? *J. Volcanol. Geotherm. Res*. 327, 407–415. doi: 10.1016/j.jvolgeores.2016.09.003

Arámbula-Mendoza, R., Lesage, P., Valdés-González, C., Varley, N., Reyes-Dávila, G., and Navarro, C. (2011). Seismic activity that accompanied the effusive and explosive eruptions during the 2004–2005 period at Volcán de Colima, Mexico. *J. Volcanol. Geotherm. Res*. 205, 30–46. doi: 10.1016/j.jvolgeores.2011.02.009

Barquero, J., and Segura, J. (1983). La actividad del volcán Rincón de la Vieja. *Bol. Vulcanol.* 13, 5–10.

Boatwright, J. (1980). A spectral theory for circular seismic sources: Simple estimates of source dimension, dynamic stress drop, and radiated seismic energy. *Bull. Seismol. Soc. Am.* 70, 1–27.

Boudon, G., Rancon, J. P., Kieffer, G., Soto, G. J., Traineau, H., and Rossignol, J. C. (1996). Les eruptions de 1966–1970 et 1991–1992 du volcan Rincón de la Vieja, Costa Rica: exemple d'activité recurrente d'un systéme hydromagmatique. *C.R. Acad. Sci. Paris* 322-IIa, 101–108.

Brandes, C., Astorga, A., Back, S., Littke, R., and Winsemann, J. (2007). Deformation style and basin-fill architecture of the offshore Limón back-arc basin (Costa Rica). *Marine Petrol. Geol.* 24, 277–287, doi: 10.1016/j.marpetgeo.2007.03.002

Browne, P. R. L., and Lawless, J. V. (2001). Characteristics of hydrothermal eruptions, with examples from New Zealand and elsewhere. *Earth Sci. Rev*. 52, 299–331. doi: 10.1016/S0012-8252(00)00030-1

Carmichael, I. S. E., and Ghiorso, M. S. (1986), Oxidation-reduction relations in basic magma: a case for homogeneous equilibria. *Earth Planet. Sci. Lett*. 78, 200–210. doi: 10.1016/0012-821X(86)90061-0

Carr, M. J. (1984), Symmetrical and segmented variation of physical and geochemical characteristics of the Central American volcanic front. *J. Volcanol. Geotherm. Res*. 20, 231–252.

Carr, M. J., Feigenson, M. D., and Bennett, E. A. (1990), Incompatible element and isotopic evidence for tectonic control of source mixing and melt extraction along the Central American arc. *Contrib. Mineral. Petrol*. 105, 369–380.

Christenson, B. W., Reyes, A. G., Young, R., Moebisd, A., Sherburne, S., Cole-Bakere, J., et al. (2010). Cyclic processes and factors leading to phreatic eruption events: Insights from the 25 September 2007 eruption through Ruapehu Crater Lake, New Zealand. *J. Volcanol. Geother. Res.* 191, 15–32. doi: 10.1016/j.jvolgeores.2010.01.008

Christenson, B. W., and Tassi, F. (2015). "Gases in volcanic lake environments," in *Volcanic Lakes*, eds D. Rouwet, B. W. Christenson, F. Tassi, and J. Vandemeulebrouck (Heidelberg: Springer).

De la Cruz-Reyna, S., and Reyes-Davila, G. A. (2001). A model to describe precursory material-failure phenomena: applications to short-term forecasting at Colima volcano, Mexico. *Bull. Volcanol*. 63, 297–308. doi: 10.1007/s004450100152

de Moor, J. M., Aiuppa, A., Avard, G., Wehrmann, H., Dunbar, N., Muller, C., et al. (2016b). Turmoil at turrialba volcano (Costa Rica): degassing and eruptive processes inferred from high-frequency gas monitoring. *J. Geophys. Res. Solid Earth* 121, 5761–5775. doi: 10.1002/2016JB013150

de Moor, J. M., Aiuppa, A., Pacheco, J., Avard, G., Kern, C., Liuzzo, M., et al. (2016a). Short-period volcanic gas precursors to phreatic eruptions: Insights from Poás Volcano, Costa Rica. *Earth Planet. Sci. Lett.* 442, 218–227. doi: 10.1016/j.epsl.2016.02.056

de Moor, J. M., Kern, C., Avard, G., Muller, C., Aiuppa, A., Saballos, A., et al. (2017). A new sulfur and carbon degassing inventory for the southern central american volcanic arc: the importance of accurate time-series data sets and possible tectonic processes responsible for temporal variations in arc-scale volatile emissions. *Geochem. Geophys. Geosystems.* 18, 4437–4468. doi: 10.1002/2017GC007141

Delmelle, P., and Bernard, A. (2015). "The remarkable chemistry of sulfur in volcanic acid crater lakes: a scientific tribute to Bokuichiro Takano and Minoru Kusakabe," in *Volcanic Lakes,* eds D. Rouwet, F. Tassi J. Vandemeulebrouck, and B. Christenson (Berlin: Springer), 238–259. doi: 10.1007/978-3-642-36833-2_10

DeMets, C. (2001). A new estimate for present- day Cocos-Caribbean plate motion: Implication for slip along the Central American volcanic arc. *Geophys. Res. Lett*. 28, 4043–4047. doi: 10.1029/2001GL013518

DeMets, C., Gordon, R. G., and Argus, D. F. (2010). Geologically current plate motions. *Geophys. J. Int.* 181, 1–80. doi: 10.1111/j.1365-246X.2009.04491

Di Napoli, R., Federico, C., Aiuppa, A., D'Antonio, M., , and Valenza, M. (2013). Quantitative models of hydrothermal fluid–mineral reaction: the Ischia case, *Geochim. Cosmochim. Acta* 105, 108–129. doi: 10.1016/j.gca.2012.11.039

Fischer, T. P., Ramírez, C., Mora-Amador, R. A., Hilton, D. R., Barnes, J. D., Sharp, Z. D., et al. (2015). Temporal variations in fumarole gas chemistry at Poas volcano, Costa Rica. *J. Volcanol. Geotherm. Res*. 294, 56–70. doi: 10.1016/j.jvolgeores.2015.02.002

Gherardi, F., Panichi, C., Yock, A., and Gerardo-Abaya, J. (2002). Geochemistry of the surface and deep fluids of the Miravalles volcano geothermal system (Costa Rica). *Geothermics* 31, 91–128. doi: 10.1016/S0375-6505(01)00030-X

Giggenbach, W. F. (1987). Redox processes governing the chemistry of fumarolic gas discharges from White Island, New Zealand. *Appl. Geochem*. 2, 141–161.

Giggenbach, W. F. (1996). "Chemical composition of volcanic gas," in *IAVCEI-UNESCO: Monitoring and Mitigation of Volcanic Hazards*, ed R. Tilling (Berlin: Springer), 221–256.

Giggenbach, W. F., and Correales, R. S. (1992). Isotopic and chemical composition of water and steam discharges from volcanic-magmatic-hydrothermal systems of the Guanacaste geothermal province, Costa Rica. *Appl. Geochem*. 7, 309–332.

Global Volcanism Program, (2017). "Report on Rincon de la Vieja (Costa Rica)," in *Bulletin of the Global Volcanism Network, 42:8 Smithsonian Institution*, ed E. Venzke (Washington, DC: Global Volcanism Program).

Gunawan, H., Caudron, C., Pallister, J., Primulyana, S., Christenson, B., McCausland, W., et al. (2016). New insights into KawahIjen's volcanic system from the wet volcano workshop experiment. *Geol. Soc. Lond. Spec. Publ.* 437, 35–56. doi: 10.1144/SP437.7

Hasselle, N., Rouwet, D., Aiuppa, A., Jácome-Paz, M. P., Pfeffer, M., Taran, Y., et al. (2018). Sulfur degassing from steam-heated crater lakes: El Chichón (Chiapas, Mexico) and Víti (Iceland). *Geophys. Res. Lett*. 45, 7504–7513. doi: 10.1029/2018GL079012

Hurst, A. W., Bibby, H. M., Scott, B. J., and McGuiness, M. J. (1991). The heat source of ruapehu crater lake; deductions from the energy and mass balances. *J. Volcanol. Geother. Res.* 46, 1–11.

Kempter, K. (1997). *Geologic evolution of the Rincón de la Vieja volcanic complex, northwestern Costa Rica - 159 págs.* Ph. D. Thesis. University of Texas, Austin, TX.

Kempter, K. A., and Rowe, G. L. (2000). Leakage of Active Crater lake brine through the north flank at Rincon de la Vieja volcano, northwest Costa Rica, and implications for crater collapse. *J. Volcanol. Geother. Res.* 97, 143–159. doi: 10.1016/S0377-0273(99)00181-X

Kusakabe, M., Komoda, Y., Takano, B., and Abiko, T. (2000). Sulfur isotopic effects in the disproportionation reaction of sulfur dioxide in hydrothermal fluids: implications for the δ34S variations of dissolved bisulfate and elemental sulfur from active crater lakes. *J. Volcanol. Geotherm. Res.* 97, 287–307. doi: 10.1016/S0377-0273(99)00161-4

Lewicki, J. L., Kelly, P. J., Bergfeld, D., Vaughan, R. G., and Lowenstern, J. B. (2017). Monitoring gas and heat emissions at Norris Geyser Basin, Yellowstone National Park, USA based on a combined eddy covariance and Multi-GAS approach. *J. Volcanol. Geother. Res.* 347, 312–326. doi: 10.1016/j.jvolgeores.2017.10.001

Mastin, L. G., and Witter, J. B. (2000). The hazards of eruptions through lakes and seawater. *J. Volcanol. Geother. Res.* 97, 195–214. doi: 10.1016/S0377-0273(99)00174-2

Molina, F., and Martí, J. (2016). The Borinquen geothermal system (Cañas Dulces caldera, Costa Rica). *Geothermics* 64, 410–425. doi: 10.1016/j.geothermics.2016.07.001

Molina, F., Martì J., Aguirre, G., Vega, E., and Chavarria, L. (2014). Stratigraphy and structure of the Canas Dulces caldera (Costa Rica). *Geol. Soc. Am. Bull.* 126, 1448–1466. doi: 10.1130/B31012.1

Moretti, R., Papale, P., and Ottonello, G. (2003). A model for the saturation of C–O–H–S fluids in silicate melts. *Geol. Soc. Lond. Spec. Publ.* 213, 81–101. doi: 10.1144/GSL.SP.2003.213.01.06

Ohmoto, H., and Lasaga, A. C. (1982). Kinetics of reactions between aqueous sulfates and sulfides in hydrothermal systems. *Geochim. Cosmochim. Acta* 46, 1727–1745.

Oikawa, T., Yoshimoto, M., Nakada, S., Maeno, F., Komori, J., and Shimano, T. (2016). Reconstruction of the 2014 eruption sequence of Ontake Volcano from recorded images and interviews. *Earth Planet. Space* 68:79. doi: 10.1186/s40623-016-0458-5

Oppenheimer, C. (1992). Sulphur eruptions at Volcan Poas, Costa Rica. *J. Volcanol. Geother. Res.* 49, 1–21.

OVSICORI (Observatorio Vulcanologico y Sismologico de Costa Rica), (1995). *Actividad Eruptiva del Volcan Rincon de la Vieja durante los dias 6–13 de noviembre, 1995.* Open report, OVSI- CORI-UNA, p. 42.

Pasternack, G. B., and Varekamp, J. C. (1997). Volcanic lake systematics I. Physical constraints. *Bull. Volcanol*. 58, 528–538.

Pering, T. D., Tamburello, G., McGonigle, A. J. S., Aiuppa, A., Cannata, A., Giudice, G., et al. (2014). High time resolution fluctuations in volcanic carbon dioxide degassing from Mount Etna. *J. Volcanol. Geotherm. Res.* 270, 115–121. doi: 10.1016/j.jvolgeores.2013.11.014

Rouwet, D., and Morrissey, M. M. (2015). "Mechanisms of crater lake breaching eruptions," in *Volcanic Lakes*, eds D. Rouwet, B. W. Christenson, F. Tassi, and J. Vandemeulebrouck (Heidelberg: Springer).

Rye, R. O. (2005). A review of the stable-isotope geochemistry of sulfate minerals in selected igneous environments and related hydrothermal systems. *Chem. Geol.* 215, 5–36. doi: 10.1016/j.chemgeo.2004.06.034

Shinohara, H., Hirabayashi, J., Nogami, K., and Iguchi, M. (2011). Evolution of volcanic gas composition during repeated culmination of volcanic activity at Kuchinoerabujima volcano, Japan. *J. Volcanol. Geotherm. Res.* 202, 107–116. doi: 10.1016/j.jvolgeores.2011.01.011

Shinohara, H., Yoshikawa, S., and Miyabuchi, Y. (2015). "Degassing activity of a volcanic crater lake: volcanic plume measurements at the yudamari crater lake, aso Volcano, Japan," in *Volcanic Lakes, Advances in Volcanology*, eds D. Rouwet, B. Christenson, F. Tassi, and J. Vandemeulebrouck (Berlin; Heidelberg: Springer).

Stix, J., and de Moor, J. M. (2018). Understanding and forecasting phreatic eruptions driven by magmatic degassing. *Earth Planet. Space* 70:83. doi: 10.1186/s40623-018-0855-z

Symonds, R. B., Gerlach, T. M., and Reed, M. H. (2001). Magmatic gas scrubbing: implications for volcano monitoring. *J. Volcanol. Geother. Res.* 108, 303–341. doi: 10.1016/S0377-0273(00)00292-4

Symonds, R. B., Janik, C. J., Evans, W. C., Ritchie, B. E., Counce, D., Poreda, R. J., et al. (2003). Scrubbing masks magmatic degassing during repose at Cascade-Range and Aleutian-Arc volcanoes. *US Geol. Surv. Open File Rep.* 3, 3–435. Available online at: http://pubs.usgs.gov/of/2003/0435/

Takano, B., Ohsawa, S., and Glover, R. B. (1994). Surveillance of Ruapehu Crater Lake, New Zealand, by aqueous polythionates. *J. Volcanol. Geother. Res.* 60, 29–57. doi: 10.1016/0377-0273(94)90096-5

Tamburello, G. (2015). Ratiocalc: Software for processing data from multicomponent volcanic gas analyzers. *Comput. Geosci.* 82, 63–67. doi: 10.1016/j.cageo.2015.05.004

Tamburello, G., Agusto, M., Caselli, A., Tassi, F., Vaselli, O., Calabrese, S., et al. (2015). Intense magmatic degassing through the lake of Copahue volcano, 2013–2014. *J. Geophys. Res. Solid Earth* 120, 6071–6084. doi: 10.1002/2015JB012160

Tassi, F., Vaselli, O., Capaccioni, B., Giolito, C., Duarte, E., Fernandez, E., et al. (2005), The hydrothermal-volcanic system of Rincón de la Vieja volcano (Costa Rica): a combined (inorganic and organic) geochemical approach to understanding the origin of the fluid discharges and its possible application to volcanic surveillance. *J. Volcanol. Geother. Res.* 148, 315–333. doi: 10.1016/j.jvolgeores.2005.05.001

Tassi, F., Vaselli, O., Fernandez, E., Duarte, E., Martinez, M., Delgado, A., et al. (2009). Morphological and geochemical features of crater lakes in Costa Rica: an overview. *J. Limnol.* 68, 193–205. doi: 10.3274/JL09-68-2-04

Varekamp, J. C., Pasternack, G. B., and Rowe, G. L. Jr. (2000). Volcanic lake systematics II. Chemical constraints. *J. Volcanol. Geother. Res.* 97, 161–179. doi: 10.1016/S0377-0273(99)00182-1

Conflict of Interest Statement: The authors declare that the research was conducted in the absence of any commercial or financial relationships that could be construed as a potential conflict of interest.